Article

Molecular Cell

The Biogenesis of SRP RNA Is Modulated by an RNA Folding Intermediate Attained during Transcription

Graphical Abstract

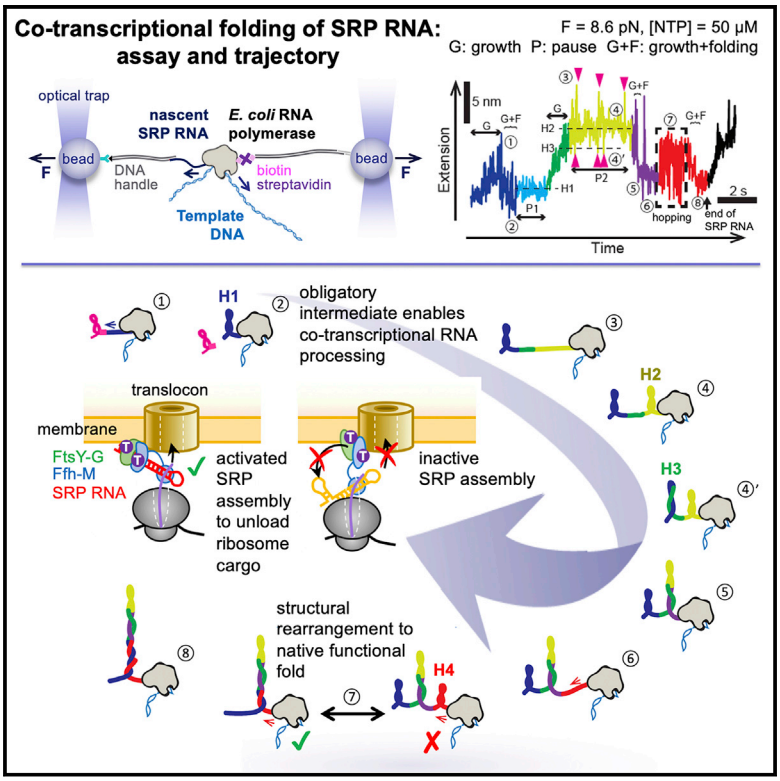

Highlights

- SRP RNA exhibits robust co-transcriptional folding invariant to transcription rates
- SRP RNA adopts a non-native obligatory intermediate prior to its functional fold
- The obligatory intermediate enables SRP RNA maturation during early transcription
- Altering the non-native-to-native transition in SRP RNA impacts cell viability

Authors

Shingo Fukuda, Shannon Yan, Yusuke Komi, Mingxuan Sun, Ronen Gabizon, Carlos Bustamante

Correspondence

shingof0617@gmail.com (S.F.), shannonyan@berkeley.edu (S.Y.), carlosb@berkeley.edu (C.B.)

In Brief

SRP RNA begins to fold during its synthesis by RNA polymerase. Fukuda et al. find that SRP RNA exhibits a robust co-transcriptional folding pattern, including (1) the initial formation of a non-native obligatory intermediate that enables RNA maturation and (2) its eventual resolution into the native fold that confers SRP functionality.

Fukuda et al., 2020, Molecular Cell 77, 1–10
January 16, 2020 Published by Elsevier Inc.
https://doi.org/10.1016/j.molcel.2019.10.006

Please cite this article in press as: Fukuda et al., The Biogenesis of SRP RNA Is Modulated by an RNA Folding Intermediate Attained during Transcription, Molecular Cell (2019), https://doi.org/10.1016/j.molcel.2019.10.006

Molecular Cell
Article

The Biogenesis of SRP RNA Is Modulated by an RNA Folding Intermediate Attained during Transcription

Shingo Fukuda,[1,2,3,12,*] Shannon Yan,[1,4,12,*] Yusuke Komi,[1,5] Mingxuan Sun,[1,4] Ronen Gabizon,[1] and Carlos Bustamante[1,4,6,7,8,9,10,11,13,*]
[1]Institute for Quantitative Biosciences-QB3, University of California, Berkeley, Berkeley, CA, USA
[2]Okazaki Institute for Integrative Bioscience and Institute for Molecular Science, National Institutes of Natural Science, Tokyo, Japan
[3]Nano Life Science Institute (WPI-NanoLSI), Kanazawa University, Kanazawa 920-1192, Japan
[4]Department of Molecular and Cell Biology, University of California, Berkeley, Berkeley, CA, USA
[5]Laboratory for Protein Conformation Diseases, RIKEN Center for Brain Science, Wako, Saitama, Japan
[6]Jason L. Choy Laboratory of Single-Molecule Biophysics, University of California, Berkeley, Berkeley, CA, USA
[7]Biophysics Graduate Group, University of California, Berkeley, Berkeley, CA, USA
[8]Department of Chemistry, University of California, Berkeley, Berkeley, CA, USA
[9]Department of Physics, University of California, Berkeley, Berkeley, CA, USA
[10]Howard Hughes Medical Institute, University of California, Berkeley, Berkeley, CA, USA
[11]Kavli Energy Nanoscience Institute, University of California, Berkeley, Berkeley, CA, USA
[12]These authors contributed equally
[13]Lead Contact
*Correspondence: shingof0617@gmail.com (S.F.), shannonyan@berkeley.edu (S.Y.), carlosb@berkeley.edu (C.B.)
https://doi.org/10.1016/j.molcel.2019.10.006

SUMMARY

The signal recognition particle (SRP), responsible for co-translational protein targeting and delivery to cellular membranes, depends on the native long-hairpin fold of its RNA to confer functionality. Since RNA initiates folding during its synthesis, we used high-resolution optical tweezers to follow in real time the co-transcriptional folding of SRP RNA. Surprisingly, SRP RNA folding is robust to transcription rate changes and the presence or absence of its 5′-precursor sequence. The folding pathway also reveals the obligatory attainment of a non-native hairpin intermediate (H1) that eventually rearranges into the native fold. Furthermore, H1 provides a structural platform alternative to the native fold for RNase P to bind and mature SRP RNA co-transcriptionally. Delays in attaining the final native fold are detrimental to the cell, altogether showing that a co-transcriptional folding pathway underpins the proper biogenesis of function-essential SRP RNA.

INTRODUCTION

Nascent RNA transcripts, like their protein counterparts, begin to fold during their synthesis, before the entire sequence is completed and released from RNA polymerase (RNAP) (Al-Hashimi and Walter, 2008; Pan and Sosnick, 2006; Perales and Bentley, 2009). This scenario suggests that the co-transcriptional folding landscape of RNA may differ from that of full-length RNA and possibly contain alternative folding intermediates. The set of accessible intermediates may be particularly significant for functional RNAs, whose essential cellular activity hinges tightly on the attainment of specific folds. The mechanism underlying co-transcriptional RNA folding has been investigated intensely by means of biochemical bulk assays as well as computational methods (Chao et al., 1995; Heilman-Miller and Woodson, 2003; Lewicki et al., 1993; Nechooshtan et al., 2014; Palangat et al., 1998; Pan et al., 1999; Wong et al., 2005, 2007; Zhang and Landick, 2016; Zhao et al., 2011). Single-molecule force spectroscopy was also employed to monitor the folding of a *pbuE* adenine riboswitch and its conformational switching upon ligand binding (Frieda and Block, 2012). However, the roles of the co-transcriptional intermediates in the functionality of essential RNAs and the viability of the cell have not been addressed in depth.

The RNA core of the signal recognition particle (SRP), a highly conserved protein biogenesis machinery, is a suitable model system to study the co-transcriptional folding of RNA (Doudna and Batey, 2004; Keenan et al., 2001). This 114-nt SRP RNA from *Escherichia coli* is known to fold into a simple, ~50-bp-long functional hairpin. It is in this native fold that SRP RNA orchestrates elaborate and critical conformational rearrangements of the SRP proteins (Ffh and FtsY), which activate SRP for co-translational protein delivery to the appropriate translocation machineries in cell membranes (Figure 1A) (Akopian et al., 2013). Specifically, SRP RNA recruits Ffh with pico-molar affinity to its hairpin tip-proximal stem (next to the hairpin tetra-loop); the complex then targets ribosome cargos displaying specific nascent polypeptide chains. Next, the G-domain of Ffh (G for GTPase) associates with the G-domain of the membrane-bound SRP receptor protein FtsY, thereby bringing cargos into the vicinity of translocons. To initiate cargo unloading, the G-domains

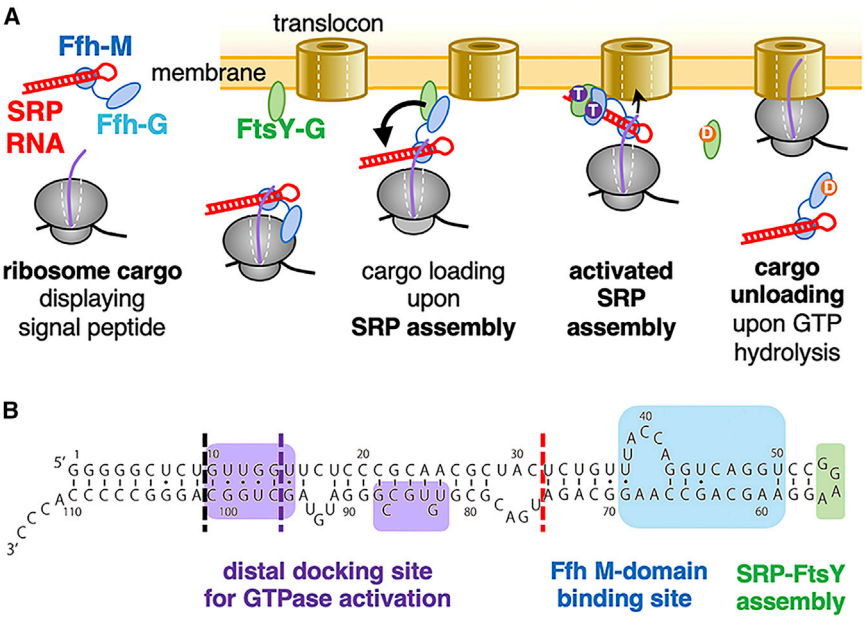

Figure 1. Protein-Targeting Activity Orchestrated by the Native Long-Hairpin Fold of SRP RNA

(A) Left to right: the signal recognition particle (SRP) in *E. coli* is composed of SRP RNA (red) and an SRP protein, Ffh (blue), whose M-domain binds to RNA hairpin-tip proximal stem. This ribonucleoprotein complex recognizes nascent signaling peptides (purple) displayed on the ribosome cargos (gray), which are then brought to the translocons (brown barrels). The SRP:cargo complex first interacts with the membrane-bound SRP receptor protein, FtsY (green), via the G-domains of Ffh and FtsY. Next, the two G-domains swing from the SRP RNA hairpin tip (black arrow) and dock onto the hairpin-tip distal stem. This conformational rearrangement is the crucial checkpoint that triggers GTP hydrolysis on the two proteins (purple dot for GTP; orange for GDP) and activates cargo unloading to the translocon, through which the synthesized polypeptide is transported.

(B) The native, functional long-hairpin fold of 114-nt-long SRP RNA from *E. coli*. The hairpin-tip proximal stem where Ffh M-domain binds is highlighted in blue, and the hairpin tetra-loop region where the SRP-FtsY assembly initially interacts is in green. The hairpin-tip distal stem highlighted in purple is the G-domain docking site, which is essential for SRP protein-targeting activity. Blunt-ended truncations (colored dash lines) on the long-hairpin fold of SRP RNA incrementally lower SRP GTPase activity and eventually impair SRP-protein-targeting functionality (black, no impact; purple, lowered GTPase activity; red, loss of activity).

must rearrange their conformation, swinging together from the hairpin tetra-loop end to dock on the hairpin tip-distal stem, which comprises nucleotides 10–15 and 96–101 of the SRP RNA (Heilman-Miller and Woodson, 2003; Jagath et al., 2001; Peterson and Phillips, 2008; Shen et al., 2013; Siu et al., 2007). This docking configuration subsequently activates guanosine triphosphate (GTP) hydrolysis and signals cargo unloading. When the distal stem of SRP RNA is shortened by more than 14 bp (Figure 1B), the docking configuration is impaired, which attenuates GTPase activity and abolishes ribosome cargo transport (Ataide et al., 2011). Therefore, the attainment of the SRP RNA native, long-hairpin fold is essential for SRP functionality.

Here we use high-resolution optical tweezers (Comstock et al., 2011; Gabizon et al., 2018; Righini et al., 2018) to follow in real time the co-transcriptional folding of 4.5S RNA, the premature form of SRP RNA—as naturally transcribed by RNAP from the *ffs* gene—with a 24-nt-long precursor sequence appended at its 5′ end, and compare it to that of mature SRP RNA (Bothwell et al., 1976; Hsu et al., 1984). We find that SRP RNA folding requires a partially folded intermediate that must later be resolved into the correct state. This intermediate raises many questions about co-transcriptional folding: does the vectorial (5′ to 3′) nature of RNA synthesis favor the folding and sequestering of the upstream RNA sequences into non-native intermediate structures? Are on-pathway folding intermediates always productive (i.e., part of the final native state), or, alternatively, can a nonproductive intermediate be on pathway (i.e., obligatory) co-transcriptionally? How does the rate at which the nascent RNA emerges from RNAP alter the folding process? Does RNAP pausing (Artsimovitch and Landick, 2000; Gabizon et al., 2018; Larson et al., 2014) play a role in determining the folding pathway? As a functional RNA transcript emerges from RNAP, do changes in the population and residence time of the molecule in intermediate states lead to any biological consequences? Hence, we also characterize *in vivo* the effect from mutant SRP RNAs with altered folding dynamics to interrogate the physiological relevance of co-transcriptional RNA folding.

RESULTS

SRP RNA Co-transcriptional Folding Is Robust

To observe how SRP RNA naturally attains its 50-bp-long hairpin functional fold, we use a high-resolution dual-trap optical tweezers to tether a single-polymerase-RNA nascent chain complex and monitor the tether end-to-end extension as the RNA emerges and folds on the surface of *E. coli* RNAP. Specifically, the RNAP-RNA complex is tethered between DNA handles and connected to a pair of surface-modified polystyrene beads manipulated by infrared (IR) laser traps (Figure 2A; STAR Methods). The nascent complex is stalled after the T7A1 promoter at a short G-less sequence located before the *ffs* gene (pre-SRP RNA, 24 + 114 nt) or before the mature, shortened version (114 nt; STAR Methods) and held under a low constant tension (8.6 pN) to permit the folding of nascent transcript. Nucleotide triphosphates (NTPs) at various concentrations (10 μM to 1 mM; K_M ~250 μM) (Harada et al., 2001) were then delivered to restart transcription. A typical co-transcriptional folding trajectory of extension versus time is shown in Figure 2B (y axis, extension in nanometers; x axis, time in seconds). The positive slope in the trajectory reflects the continuous growth of RNA (*G* in Figure 2B), while a sudden decrease (i.e., vertical drop) in tether extension reflects a folding transition (*F*). The

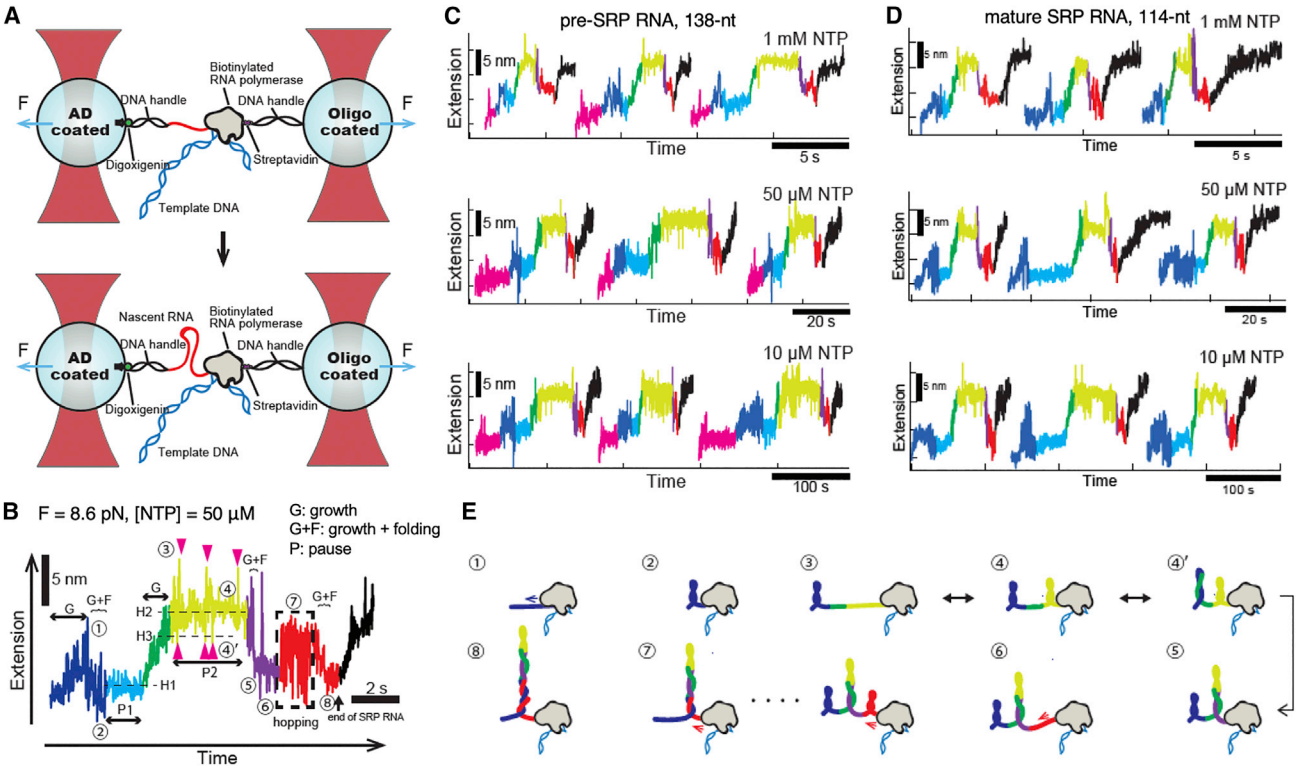

Figure 2. Robust Co-transcriptional Folding of SRP RNA Resolved by Single-Molecule Optical Tweezers

(A) An *E. coli* RNA polymerase (RNAP) elongation complex is tethered via a pair of double-stranded DNA handles and held on the optical tweezers. Active transcription at different [NTP] is monitored in real time, where the growth and folding of nascent RNA is detected as the tether extension change under constant force (STAR Methods).

(B) A representative co-transcriptional folding trajectory of SRP RNA recorded at 8.6 pN and 50 μM NTP. The positive slope in tether extension reflects the gradual growth (*G*) of nascent transcript; the horizontal segments (i.e., no change in extension over time) signify transcriptional pauses (P1 and P2). A decrease in extension indicates RNA folding (*F*), which is seen as a vertical drop in the trajectory, or a negative slope if the transcript growth and the folding occur concurrently (*G* + *F*). Hopping dynamics in the trajectory (region highlighted in red) reveal that the transcript rapidly unfolds and refolds, manifesting transitions between competing structural folds. After completing the transcription of SRP RNA encoded in the template DNA (black arrow), RNAP continues to transcript a short DNA spacer (region colored in black) before it runs off the template DNA and breaks the tether (see STAR Methods). This last stretch of monotonic/feature-less RNA extension growth serves as an ending landmark for a valid trajectory recording. See main text for assignments on intermediate folds H1, H2, and H3.

(C and D) Representative co-transcriptional folding trajectories of pre-SRP RNA (24 + 114 nt) (C) and mature SRP RNA (114 nt) (D) at different transcription rates (see timescale bar) as a function of [NTP] (n = 41, 37; F = 8.6 pN).

(E) A schematic cartoon illustrates the folding evolvement of nascent SRP RNA as it is transcribed by RNAP.

horizontal segments (i.e., tether length invariant over time) correspond to transcriptional pauses of RNAP on the template DNA (P), whereas regions of gradual negative slope in the trajectory are periods where RNA growth and folding occur concurrently (*G* + *F*) with the nascent transcript. That is, as one nucleotide newly emerges from the RNAP, it readily base pairs/condenses with another complementary nucleotide in the upstream section of the RNA nascent chain, thus leading to a shortening of the transcript extension by a total of two nucleotides.

Surprisingly, the co-transcriptional folding trajectory of SRP RNA is invariant and remains robust across three orders of magnitude change in NTP concentration (Figure 2C for three examples of pre-SRP RNA, 24 + 114 nt, n = 41; Figure 2D for mature SRP RNA, 114 nt, n = 37; also Figure S1A). Indeed, trajectories with vastly different transcription rates, all within the physiological range (i.e., from ~1 nt/s at 10 μM NTP to ~50 nt/s at 1 mM NTP), can be rescaled by their total duration to superimpose onto one another. This observation is contrary to cases wherein RNA-folding trajectories are drastically altered by heterologous polymerases from bacterial phages synthesizing *E. coli* RNAs at artificially high rates and with different transcription pausing patterns (Lewicki et al., 1993). Furthermore, Figures 2C and 2D show that the folding trajectories obtained for the precursor-bearing and the mature RNA sequences are identical, other than the fact that the former trajectory is simply appended with an extra extension feature illustrating the initial synthesis of 24-nt-long precursor fragment (highlighted in magenta). Hence, in the remainder of this study, except for places noted explicitly, we use the mature SRP RNA template (114 nt).

An Obligatory Non-native Intermediate

We find that the folding trajectories of SRP RNA consistently and reproducibly comprise three main features (Figure 2B): (1) a small hump (highlighted in dark blue); (2) two long plateaus (highlighted

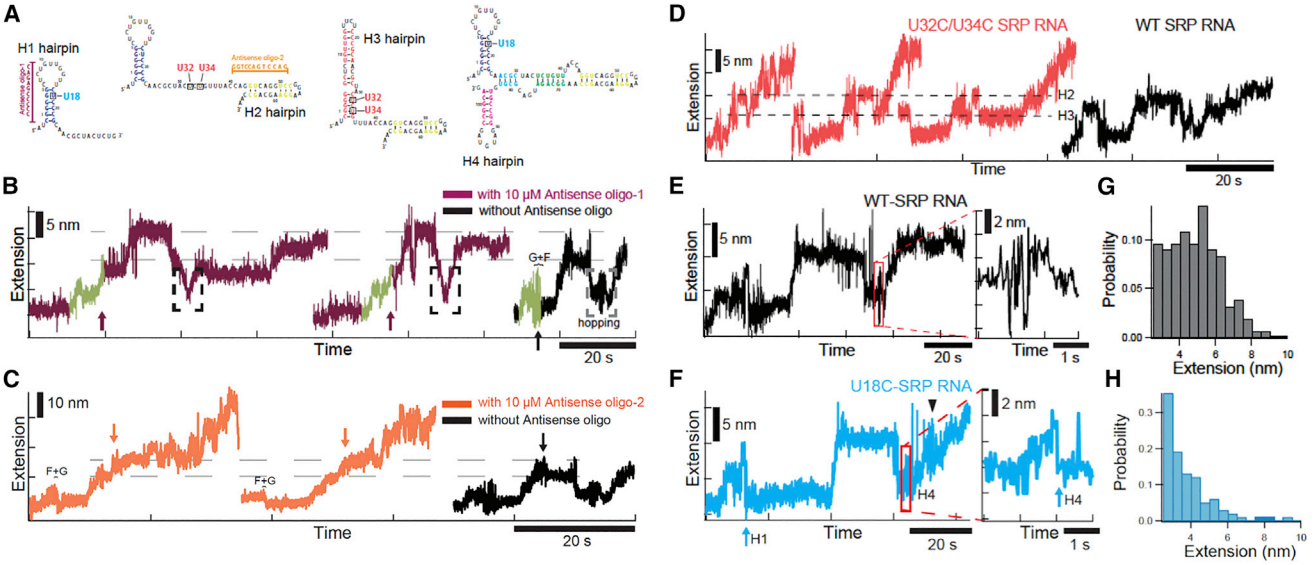

Figure 3. Modulate Co-transcriptional Folding Intermediates by Antisense Oligos and Point Mutations

(A) Structures of SRP RNA co-transcriptional folding intermediates: H1, H2, H3, and H4 hairpins. Antisense oligo-1 and oligo-2 respectively target the 5′ arms of H1 and H2. U18C mutation stabilizes H1, and U32C/U34C stabilizes H3. The self-complementary region on SRP RNA 5′ stretch sequesters the transcript 5′ end in H1 fold; the self-complementary 3′ stretch of SRP RNA, eventually base-pairing with the 5′ stretch to form the hairpin-tip distal stem, similarly sequesters the transcript 3′ end in H4.

(B and C) Representative co-transcriptional folding trajectories of wild-type SRP RNA recorded with 10 μM antisense oligo-1 (dark red) (B) and oligo-2 (orange; at 50 μM NTP) (C); the wild-type trajectory without antisense oligos (black) is shown for comparison. Oligo-1 eliminates the initial drop in extension (dark red arrows) that signifies H1 formation (*G* + *F*; highlighted in dark yellow) and the subsequent hopping dynamics (dashed-line boxes) that indicate structural rearrangements of H1 into the native fold. Oligo-2 prevents H2 folding (i.e., the hairpin tip-proximal stem in yellow; Figure 2E), thereby generating an upward-going trace absent of the middle plateau feature (orange and black arrows; gap between gray dashed lines).

(D–F) Representative co-transcriptional folding trajectories of U32C/U34C (red) (D), wild-type (black) (E), and U18C (cyan) (F) transcripts (F = 8.6 pN; 50 μM NTP). Hopping dynamics near the end of transcription (red box region in E and F) are attenuated with the U18C mutation, signifying that the structural transition toward the long-hairpin native fold becomes less favored. Instead, a hump-like feature is detected (red box zoom-in in F; similar to that of H1 formation, cyan arrows), indicating that the transcript 3′ stretch samples a small hairpin fold (H4 in A) before attaining the native fold.

(G and H) Histograms on the magnitude of hopping dynamics show that attempts to transition from H1 to the native fold is attenuated with the U18C mutant (cyan; n = 99) (H) as compared to the wild type (gray; n = 153) (G).

in light blue and yellow, respectively), where the latter one is embedded with spikes; and (3) a distinct hopping feature in RNA extension (highlighted in red) occurring just before the completion of SRP RNA synthesis (Figure 2B, black arrow). To assign the folding features in the trajectory to specific portions of the nascent RNA (see sections below), we performed additional non-equilibrium co-transcriptional folding experiments under three conditions: (1) in the presence of antisense oligos to block particular secondary structural folds (Figures 3B and 3C), (2) with transcripts harboring mutations to promote and stabilize those folds (Figures 3D–3F), and (3) under depleting NTP conditions to lengthen specific transcriptional pauses (Figures S1B and S1C). We also collected unfolding force-extension (F-X) curves to examine intermediate folds adopted by nascent transcripts of incremental length stalled on RNAP at equilibrium (Figures S2A, S2B, S2D, and S2E; STAR Methods) and RNA extension hopping experiments to interrogate folding transitions between specific intermediates at quasi-equilibrium (Figure S3; STAR Methods).

The first hump in the trajectory corresponds to the initial growth of the nascent transcript until it reaches a length of 17–20 nt, followed by a subsequent folding transition in which it forms a small intermediate hairpin, H1 not present in the native fold (Figure 2E, 2 and 8). Note that after this initial folding event, the RNA extension drops approximately to the same level as the starting point of the trajectory (Figure 2B). This initial hump for non-native-like H1 folding is present at all transcription rates tested (Figures 2C and 2D) and hence co-transcriptionally obligatory but becomes an upward slope in the presence of antisense oligo-1 (dark red traces in Figure 3B), which is complementary to the first 10 nt of SRP RNA (Figure 3A). In this case, the H1 folding is now outcompeted by the antisense oligo-1, and the RNA tether extension becomes larger (Figure 3B, difference between gray dashed lines), because the right-arm stretch of H1 remains as a single strand.

After the first intermediate hairpin (H1) forms, RNAP pauses (P1, light blue in Figure 2B), then resumes transcription for another ~55 nt (green in Figure 2B) and pauses again (P2, yellow in Figure 2B). Both pause durations increase when [UTP] (concentration, in molar, of uridine 5'-triphosphate) is selectively decreased during transcription, while the second pause, P2, also lengthens at low [GTP] (Figure S1C). To identify which U or G in the transcript sequence corresponds to P1 and P2, we performed the same real-time RNA synthesis experiments

under high tension (~22 pN) to increase the spatial resolution of the transcription trajectory and to prevent folding transitions. (Righini et al., 2018) We found that P1 occurs at U_{36} (36.2 ± 2.5 nt into transcription, indexed as the mature SRP RNA sequence; Figure S4), whereas P2 occurs around U_{82}/U_{84}—a known prominent pause site that has been shown to be suppressed by base-pairing compensating mutations U82A/A25U.(Wong et al., 2007) In the presence of these mutations, P2 shortens significantly, confirming our assignment. The $G_{73}U_{82}G_{83}$ stretch around P2 matches the consensus pause element $G_{-10}Y_{-1}G_{+1}$ described for RNAP (Vvedenskaya et al., 2014) and resulting in the strong G-pause detected at P2. As for P1, its U-rich sequence stretch $U_{34}G_{35}U_{36}U_{37}U_{38}$, and similarly the $U_{82}G_{83}U_{84}$ stretch at P2, resemble another pause-promoting element ($U_{-2}G_{-1}$) reported previously for *E. coli* RNAP (Hein et al., 2011), hence resulting in long transcriptional pauses under limiting [UTP]. Therefore, the occurrences of P1 and P2 are independent of RNA secondary structure formation, consistent with their persistence in the folding-free high-tension trajectories. We also found that these pauses do not involve backtracking of RNAP, since they are invariant to the addition of GreB, a transcription factor that rescues RNAP from backtracking pauses (Figures S1E and S1F) (Toulmé et al., 2000).

RNA-Fold Sampling and Transition to Native State

During P2, the emerged nascent transcript is ~70 nt long and spends most of the time in a partially folded state that contains the non-native intermediate hairpin H1 on the 5′ end and a second hairpin H2 ~24 nt downstream (④ in Figure 2E). Interestingly, at this point we detect upward and downward spikes of discrete sizes in RNA extension (magenta arrowheads in Figure 2B), which are different structural folds accessible and transiently visited by the newly synthesized stretch of SRP RNA (Figure 2E, yellow segment in 3). This behavior corresponds to hairpin H2 unfolding (i.e., the large extension, upward spikes observed on P2 and quickly refolding into a more compact but short-lived state, hairpin H3 (④′ in Figure 2E; the downward spikes). As before, to confirm our assignment, we specifically inhibited H2 folding with an antisense oligo-2 (Figure 3A), which renders the right-arm stretch of H2 unpaired and leads to an upward shift in extension for the P2 region of the trajectory (Figure 3C, difference between gray dashed lines). Thus, H2 constitutes the hairpin tip-proximal stem of the native fold, known to provide the essential binding site for protein Ffh to associate with SRP RNA (Figure 1B, blue-shaded region). To confirm the assignment of hairpin H3, we use specific point mutations, U32C/U34C, that should preferentially stabilize this putative state. The co-transcriptional folding trajectory recorded with these mutants demonstrates a clear lengthening of residence time in the H3 state; i.e., the downward spikes in P2 become well-resolved dwells as seen in Figure 3D (red traces).

Eventually, RNAP exits pause P2 and resumes transcription, adding nucleotides to the 3′ end of the ~70-nt-long nascent SRP RNA. In this part of the folding trajectory, however, the RNA extension exhibits a negative slope (purple region in Figure 2B), whose magnitude is [NTP] dependent, with lower [NTP] leading to shallower slopes (Figure S1A). This observation indicates that in this region, RNA growth and folding occur concurrently, wherein the newly synthesized section of RNA (~31 nt) readily base pairs with the upstream complementary single-stranded region located between the two intermediate hairpins, H1 and H2 (Figure 2E, ⑤; purple zipping with green). At this point, ~60% of the final long-hairpin native fold of SRP RNA is completed, while ~20 nt at its 5′ end are sequestered in the non-native intermediate hairpin fold H1.

As the SRP RNA continues to grow (from ~101 nt to 114 nt; Figure 2B, region in red), we observed distinct hopping in extension, reflecting the rapid folding (low extension) and unfolding (large extension) of the nearly completed transcript as it samples competing folding states. The histogram of hopping amplitude shows an average of 4.5 ± 1.5 nm and maximum at ~8 nm (Figure 3G), which corresponds to an extension gain of ~21 nt (under 8.6 pN of tension), suggesting transient multiple attempts at unfolding and resolving non-native hairpin H1. This interpretation is corroborated by the aforementioned antisense oligo-1 control experiment; when the initial formation of H1 is abolished, the hopping dynamics are eliminated near the end of transcription (black-dashed boxes in Figure 3B). These correlated features in the trajectory indicate that the hopping dynamics reflect a structural bi-stability during which the ~14-nt RNA 3′ end gradually shifts the folding equilibrium away from the state in which the RNA 5′ stretch is organized into hairpin H1 to a state in which the 5′ stretch is released to anneal with the emerging complementary 3′ stretch (Figure 2E, ⑥–⑦). The negative slope preceded by the hopping feature evidences the occurrence of such a concurrent RNA growth and folding (Figure 2B, region in red), which leads to the final native state of SRP RNA. To examine the structure attained by this completed SRP RNA, we ramped up the tension to unfold the RNA at the end of the co-transcriptional trajectory; we observed a single unfolding step of ~114 nt in extension gain (Figure S2C). This value matches the number of nucleotides involved in the SRP RNA native fold; the single cooperative unfolding transition again supports the attainment of the native long hairpin state, which contains the hairpin tip distal-stem essential for SRP's protein-targeting activity.

Co-transcriptional Maturation of SRP RNA

The co-transcriptional folding trajectory of SRP RNA, besides being robust to vastly different transcription rates, is also invariant to the presence of 24-nt 5′-precursor sequence. We hence ask whether, given its inert impact on folding, this 5′ precursor might be cleaved off sometime during transcription. In the cell, the 5′ precursor must be removed, either during or after transcription, in order to generate the 114-nt mature SRP RNA. While the field generally assumes that maturation of functional RNAs occurs after the transcripts are synthesized and released from RNAP, the exact timing of 5′ cleavage is unknown. Yet, existing studies on co-transcriptional folding of SRP RNA have been conducted mostly with the mature sequence lacking the 5′ precursor (Wong et al., 2007). The fact that the 138-nt pre-SRP RNA is not isolated from bacteria unless the processing enzyme RNase P, which is five times less abundant, is impaired, which generates a mixture of pre- and mature products, suggests an extremely rapid or co-transcriptional maturation of SRP RNA (Altman and Kirsebom, 1999; Bothwell et al., 1976;

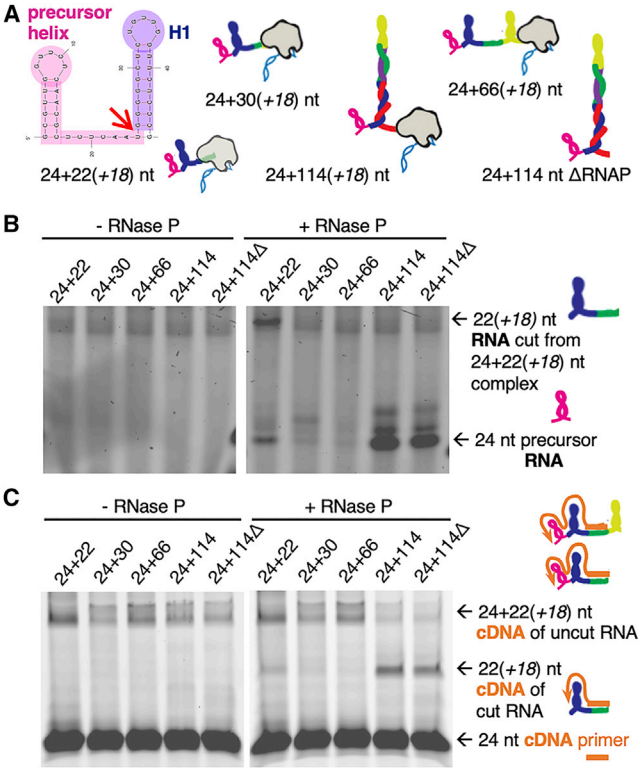

Figure 4. Obligatory Intermediate H1 Enables Maturation of SRP RNA during Early Transcription

(A) Nascent pre-SRP RNA long enough to form hairpin H1 (purple) comprises the 24-nt 5′ precursor (magenta), the 22-nt mature sequence (dark blue), and another 18 nt (green) covered by RNAP (gray). This intermediate possesses a 5′-$U_{-1}G_{+1}$/$C_{21}R_{22}$-3′ base-pair sequence at its short-stem hairpin junction (red arrow), similar to the cleavage site found in the native long-hairpin, and hence may be processed by *E. coli* RNase P. Four RNA:RNAP stalled complexes with increasing transcript length, 24 + 22 (+18), 24 + 30 (+18), 24 + 66 (+18), 24 + 114 (+18), and full-length released transcript, 24 + 114Δ, as control, are treated with RNase P to examine their propensity of co-transcriptional maturation (STAR Methods).

(B) Urea PAGE gel (7 M, 12%) resolves RNA fragments cleaved from the stalled RNAP complexes upon RNase P treatment (n = 5 replicates; negative controls in the left gel). Both the early stalled 24 + 22 (+18) complex and the full-length species, 24 + 114 (+18) and 24 + 114Δ, show a ~24-nt precursor band indicating RNase P processing. In this gel range, the ~40-nt-long 3′ side product cleaved from the 24 + 22 (+18) transcript is also detected.

(C) Urea PAGE gel (7 M, 12%) resolves cDNAs reverse transcribed from the above RNA samples using a common DNA primer (n = 5 replicates; negative controls in the left gel). Upon RNase P treatment, both the 24 + 22 (+18) complex and the full-length species, 24 + 114 (+18) and 24 + 114Δ, show two bands, a ~64-nt cDNA from the un-processed transcript and a ~40-nt cDNA from the cleaved 3′-side RNA, which is sequenced to verify the cleavage site at the 5′-$U_{-1}G_{+1}$ (STAR Methods).

Dong et al., 1996) Therefore, we looked into each intermediate detected along the SRP RNA folding trajectory for specific structural and sequence elements that match those recognized by RNase P, namely, a hairpin stem at least ~3–4 bp in size with little to no 3′ end single strand and a 5′-$U_{-1}G_{+1}$/$C_{21}R_{22}$-3′ base-pairing sequence at its hairpin junction (Figure 4A) (Li et al., 2005; McKinney et al., 2001; Peck-Miller and Altman, 1991; Sinapah et al., 2011). RNase P reportedly cuts between the U_{-1} and G_{+1} to remove the 5′ precursor and yields mature functional RNA substrates, including tRNAs (McKinney et al., 2001; Sinapah et al., 2011). We found that both the final native long-hairpin fold and the nascent obligatory non-native intermediate hairpin H1 possess the above features required for RNase P processing, and the latter may allow the possibility of co-transcriptional maturation.

To examine if RNase P indeed recognizes intermediate hairpin H1 and hence cleaves off the 24-nt 5′ precursor from the nascent SRP RNA during transcription, we prepared—in the presence/absence of RNase P—four stalled RNAP-RNA complexes displaying transcripts of various length and compared how their RNA substrates are processed by the enzyme (STAR Methods). Specifically, these four complexes correspond to evolving time points along the folding trajectory: around the time when H1 first appears (24 + 22 nt and 24 + 30 nt; Figure 2E, ②–③) and from midway (24 + 66 nt; Figure 2E, ④) to complete transcription (24 + 114 nt; Figure 2E, ⑧). We find that a small ~24-nt RNA fragment appears only when the 24 + 22-nt and 24 + 114-nt RNAP-RNA complexes are prepared in the presence of RNase P, whereas the 24 + 30-nt and 24 + 66-nt complexes show no signs of such fragments (Figure 4B). We next use a common primer, fluorophore labeled, to reverse transcribe the RNAs from these complexes. Consistently, in the presence of RNase P, the 24 + 30-nt and 24 + 66-nt complexes show only one band representing cDNAs of uncut transcripts, while both the 24 + 22-nt and 24 + 114-nt complexes show one additional lower band, which indeed is ~24 nt shorter, reflecting the 5′ truncation on the processed transcripts (Figure 4C). Judging from the fluorescence intensity ratio between the two cDNA bands, ~10% of the transcripts from the 24 + 22-nt complex are processed compared to ~90% processed from the 24 + 114-nt complex (Figure 4C; the 24 + 114-nt transcripts released from RNAP, as a control, are also processed to a similar level). Sequencing of the lower band cDNA reveals the initial bases on its RNA template 5′ end and confirms the RNase P cleavage site located between the aforementioned $U_{-1}G_{+1}$ section. These results hence demonstrate two time points at which maturation of SRP RNA is feasible: (1) during early transcription, when the nascent RNA is just long enough to form hairpin H1; and (2) when the entire SRP RNA has emerged and is available to attain the native long-hairpin fold (which is the default substrate in traditional RNase P characterization) (Peck-Miller and Altman, 1991). We speculate that the RNAP pause at the P1 site, right after H1 formation, may grant an adequate, seconds-long window for RNase P to bind H1 and process the nascent transcript co-transcriptionally.

Altered Folding Dynamics Impact Viability

The intermediate hairpin H1 on the nascent SRP RNA 5′ end, as shown above, enables the timely maturation of the RNA during initial transcription. Nevertheless, this non-active intermediate must also be resolved timely, as reflected in the hopping dynamics toward the end of folding trajectories, so that the RNA 5′ stretch sequestered by H1 can anneal with the emerging 3′ stretch to attain the activity-essential distal hairpin stem present in the SRP RNA native fold (Figure 1B). Accordingly, we wonder

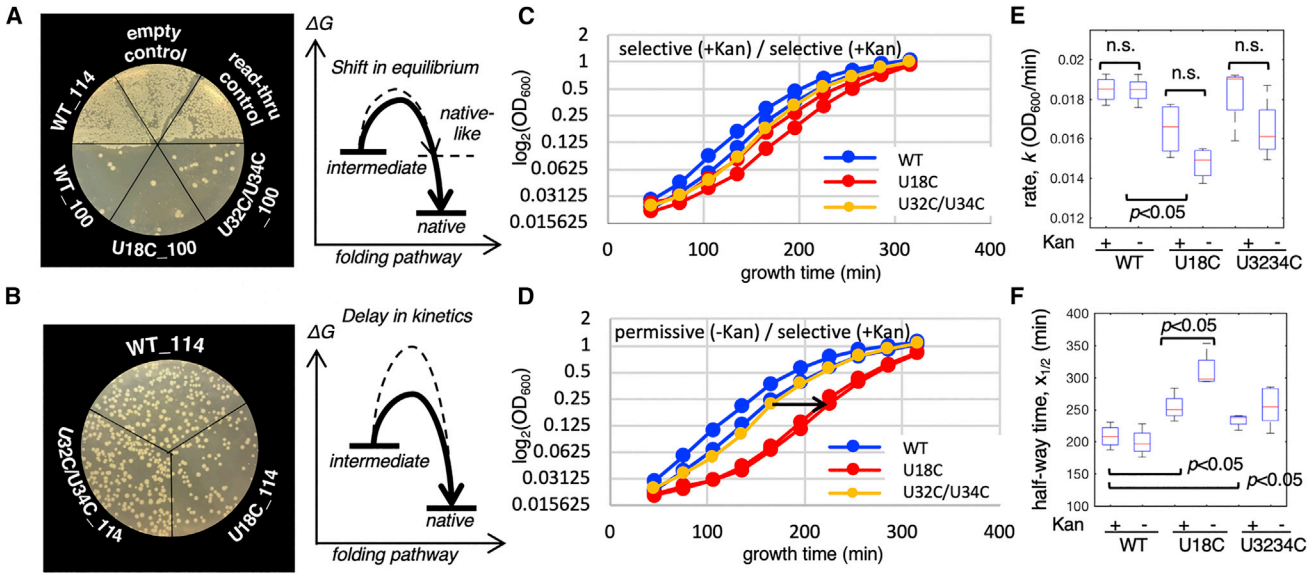

G

Toxicity of SRP RNA variants in *E. coli*

sequence / length	wild-type	U18C	U32C/U34C
truncated, 100-nt	lethal	lethal	lethal
full-length, 114-nt	normal growth	slower growth rate (*k*), longest lag phase ($x_{1/2}$)	slightly slower growth rate (*k*), longer lag phase ($x_{1/2}$)

Figure 5. Intermediate-Stabilizing Variants of SRP RNA Impact Cell Viability

(A and B) Cell viability assay of *E. coli* transformed with plasmids carrying SRP RNA variants, which shift the folding equilibrium away or delay the folding kinetics toward the native fold (n = 6 replicates; STAR Methods).

(A) Bacteria plate: transcription of full-length wild-type SRP RNA (WT_114) shows normal growth as that of the control conditions (empty plasmid and transcript read-through), whereas the 3′-truncation variants (SRP_100, U18C_100, and U32C/U34C_100) are lethal. Surviving colonies were sequenced and identified to harbor modified plasmids, which prevents transcription of specific SRP RNA variants, thereby alleviating the lethal impact (Figure S5B).

(B) Bacteria plate: for full-length SRP RNA variants containing point mutations to stabilize specific co-transcriptional folding intermediates, U32C/U34C_114 shows growth similar to that of WT_114, while U18C_114 exhibits a reduction in surviving colonies. Relative colony counts: WT_114, 100%; U32C/U34C_114, ~87%; and U18C_114, ~44%.

(C and D) Differences in toxicity of full-length SRP RNA mutants were resolved by their cell growth profiles post-selective (C) and post-permissive (D) growth condition (i.e., +Kan/+Kan and −Kan/+Kan; Kan, kanamycin; n = 5; STAR Methods). U18C_114 causes clear lengthening of the lag phase.

(E and F) Comparisons of selective growth profiles in (C) and (D). (E) Boxplot: growth rate in log phase; (F) Boxplot: halfway time reaching the stationary phase as a proxy of lag phase duration (p values calculated from two-sample t test; red mark represents the median; blue box shows the 25th–75th percentile; whisker shows maximum and minimum values; n.s., not statistically significant).

(G) Summary on the cell viability and toxicity impact of SRP RNA variants examined in this work.

what the biological consequences are when this function-critical structural rearrangement of SRP RNA is perturbed. Hence, we sought to introduce mutations in SRP RNA, either to slow down the RNA-folding kinetics or shift the equilibrium between the intermediate and the final native fold, and characterize their effect *in vivo* (Figure 5).

To delay the structural transition toward the native fold without altering the final equilibrium, we employ point mutations to lengthen the lifetime of specific co-transcriptional intermediates, such as the obligatory H1 hairpin stabilized by U18C (U18C_114; Figure 3F) and intermediate H3 by U32C/U34C (U32C/U34C_114; Figure 3D). The final folding state of these point mutant full-length transcripts has been verified to be identical as that of the wild-type full-length SRP RNA (WT_114), where they readily acquire *in vitro* the same native long-hairpin fold that exhibits comparable stability as that of the wild-type transcript and unwinds cooperatively in a single step (Figures S2G and S2H).

To shift the equilibrium away from the native fold, on the other hand, we use 3′-truncated mutants (WT_100, U18C_100, U32C/U34C_100), because according to the folding trajectories, the incomplete ~100-nt transcript rapidly transitions between the H1-bearing and native-like folds and attains comparable populations (40% and 60%; Figure S3C). Note that this native-like fold (i.e., the partial-native fold [PN] in Figure S3C) acquires the minimal G-domain docking site in the hairpin-tip distal stem (purple-highlighted region in Figure 1B), which is essential for SRP activity. Combining truncation and specific point mutations

allows us to further bias the folding equilibrium toward the H1-bearing form (e.g., 89.8% and 10.2% with U18C_100; Figure S2H).

Preparation of plasmids harboring these potentially toxic SRP RNA variants is done with a special *E. coli* strain, which tightly represses transcription of genes governed under specific promoter/operator elements (see STAR Methods; Figure S5A).(Lutz and Bujard, 1997) Next, a standard BL21 strain (since knockout of SRP RNA is inviable) is transformed with these plasmids to overexpress specific SRP RNA variants, while the endogenous 4.5S RNA is still transcribed by *E. coli* polymerase and processed by RNase P. It is known that the endogenous SRP RNA is in four times excess of the SRP protein Ffh (Jensen et al., 1994) and that the exogenous transcripts outnumber the endogenous ones. Hence, in the *in vivo* experiments, we expect that the majority of Ffh to be bound/sequestered by the SRP RNA variants (i.e., associated with the hairpin tip-proximal stem shown in Figure 1B). Accordingly, for different transcript variants, their ability to rearrange non-native intermediates (e.g., resolving hairpin H1 hairpin) into the native long-hairpin fold determines the competency of SRP complex and ultimately the cell viability.

As shown in Figure 5A, synthesis of exogenous full-length wild-type SRP RNA (WT_114) has no impact on cell viability, yielding normal growth similar to that seen with the empty plasmid control. In contrast, transcription of truncated SRP RNAs is lethal to *E. coli*, with few colonies surviving (bottom half: WT_100, U18C_100, U32C/U34C_100). We sequenced the few colonies surviving in the SRP RNA variant experiments and found that these bacteria harbored plasmids with either mutations or truncations in the promoter or terminator (Figure S5B), which prevent the precise synthesis of the intended transcripts and likely alleviate the lethal impact of those plasmids. Indeed, the terminator-omitting/read-through plasmid control (Figure 5A), though inserted with a truncated variant (WT_100), showed no deterioration of viability. Interestingly, it has been reported that when the SRP RNA hairpin-distal stem are truncated by ~10-bp (black-dashed line in Figure 1B)—namely, shortening both the 5′ and 3′ ends—SRP activity remains unaffected.(Shen et al., 2013) In other words, removing the last 14 nt on the SRP RNA 3′ end does not take away any of the nucleotides that form the essential G-domain docking site in the native long-hairpin fold. Therefore, it is the intact 5′ stretch present in the asymmetrically truncated 100-nt-long transcripts that tips the folding equilibrium of SRP RNA away from the native fold (e.g., from 100% population to 60% with the wild-type sequence) and is sufficient to render a lethal phenotype.

As for the SRP RNA full-length variants that alter folding kinetics, while U32C/U34C appears indistinguishable to that of wild type in the cell viability plate assay, U18C exhibits a moderate reduction in surviving colony counts (Figure 5B); this decline is aggravated under stress condition (e.g., high-salt growth medium; Figure S5C). Differences in toxicity of these point mutants are then evaluated by their plasmid loss in transformed cells under selective versus antibiotic-free (permissive) growth conditions and their subsequent recovery growth profiles under selection (STAR Methods) (Chen et al., 2017). We find that both point mutants, compared to wild type, exhibit a significant lengthening in the lag phase during growth (Figure 5F), indicating their impact in delaying cell maturation, which requires efficient protein production as well as protein delivery by SRP complexes before cells can divide and multiply in the log phase. Moreover, consistent with the above viability assay, U18C is the more toxic variant, because it also causes a slower growth rate in log phase (Figure 5E) and a tendency to rid of the variant-containing plasmid, as seen with the clear difference in lag phase between the selective and permissive growth condition (U18C+ and U18C−; Figure 5F). These observations hence demonstrate that kinetically delaying folding transitions for SRP RNA to attain its functional native fold in turn modulates cell growth.

DISCUSSION

Using a broad set of tools, from optical tweezers to *in vitro* and *in vivo* assays, we uncover how the co-transcriptional folding pathway of SRP RNA directs the attainment of its functional native form. An obligatory folding intermediate adopted during early transcription both enables the maturation of SRP RNA and resists alternative structural rearrangements to secure the attainment of the native form and cellular functionality. Specifically, the non-native intermediate H1 of SRP RNA persists throughout most of the co-transcriptional folding trajectory until the RNA 3′ end emerges and competes to anneal with the RNA 5′ end sequestered in H1, forming the activity-essential distal stem in the final long-hairpin fold of SRP RNA. Toehold-mediated RNA strand displacement is a thermodynamically feasible mechanism for the RNA 3′ end single strand to invade and resolve H1 (Zhang and Winfree, 2009). During toehold invasion, various stretches of the 3′ single-strand sample alternative base-pairing interactions with the loop region of H1 until a strong enough hybridization is established, compensating for the entropy cost of bringing the RNA ends together, to eventually attain complete strand displacement. The large-scale hopping dynamics observed in the co-transcriptional folding trajectory (Figure 2B) most likely reflect those transient toeholding attempts between the two ends on SRP RNA. Finally, the folding trajectories presented here have been obtained *in vitro* and, therefore, it is possible that some of the details of these trajectories may be modified *in vivo* through interactions with other cellular components. Nonetheless, we note that the predictions derived from the single-molecule *in vitro* experiments about the possible effects of SRP RNA mutants on cell viability are indeed validated in the cell experiments, suggesting that the *in vivo* milieu does not alter significantly the essential features of the folding trajectories presented here.

Future work may elucidate the present or vestigial adaptive advantage of the SRP RNA 5′ precursor, which does not alter the folding trajectory and can be removed during early transcription. Furthermore, the robust folding pathway for SRP RNA, pacing its maturation and directing the proper attainment of its native fold, suggests an elegant strategy to devise RNAs whose functionalities (such as riboswitches, transcriptional terminators, and pausing elements) evolve over time by co-transcriptionally transitioning through sequential functional folds. We also envision that co-transcriptional modulation on

RNA folding and function in other essential RNAs could be targeted by antisense therapeutics to further regulate cellular processes.

STAR★METHODS

Detailed methods are provided in the online version of this paper and include the following:

- KEY RESOURCES TABLE
- LEAD CONTACT AND MATERIALS AVAILABILITY
- METHOD DETAILS
  - Optical Tweezers
  - SRP RNA Encoded Template DNA
  - DNA Handle
  - Bead Surface Functionalization
  - Recombinant Proteins
  - Real-Time Co-transcriptionalFolding of Nascent RNA
  - Force-Extension (F-X) Curve Measurements of Truncated and Full-Length SRP RNA on the Surface of RNA Polymerase
  - Force-Extension (F-X) Curve Measurements of Truncated and Full-Length SRP RNA in Isolation
  - Unit Conversion of Transcription Trajectories Recorded in Nanometers into Nucleotides
  - RNase P Processing Assay
  - Plasmid Constructs for Cell Viability Experiments
  - CompletePlasmid Sequence of pZE21_wtSRP_FL_rrnC
  - Cell Viability Plate Assay
  - Recovery/Post-Relaxation Growth Rate
- QUANTIFICATION AND STATISTICAL ANALYSIS
- DATA AND CODE AVAILABILITY

SUPPLEMENTAL INFORMATION

Supplemental Information can be found online at https://doi.org/10.1016/j.molcel.2019.10.006.

ACKNOWLEDGMENTS

We thank L. Alexander for critical reading of the manuscript, L. Wee for sharing expertise on biochemistry assay developments, and all members of Bustamante laboratory for discussion. We also acknowledge J. Lucks, A. Yu, and E. Strobel at Northwestern University and V. Gopalan and L. Lai at Ohio State University for comments and material sharing. The pZE21 vector used in the cell experiments is a gift from A. Flamholz (Savage lab at University of California, Berkeley). This research was supported by NIH grant R01GM032543 (instrumentation and biochemistry) and the Nanomachine program (KC1203) funded by the Office of Basic Energy Sciences of the U.S. Department of Energy (DOE) contract DE-AC02-05CH11231 (data analysis algorithms). S.F. acknowledges support from the MEXT/JSPS Grants-in-Aid for Scientific Research (JP15K17889).

AUTHOR CONTRIBUTIONS

Conceptualization, S.Y. and S.F.; Methodology, S.F. and S.Y.; Investigation, S.F., S.Y., and Y.K.; Writing – Original Draft, S.Y., S.F., R.G. and C.B.; Writing – Review & Editing, S.Y., S.F., and C.B.; Funding Acquisition, C.B.; Resources, S.F., S.Y., R.G., and M.S.; Supervision, C.B.

DECLARATION OF INTERESTS

The authors declare no competing interests.

Received: August 18, 2018
Revised: August 29, 2019
Accepted: October 4, 2019
Published: November 6, 2019

SUPPORTING CITATIONS

The following reference appears in the Supplemental Information: Chen et al. (2013).

REFERENCES

(2005). Rapid amplification of 5′ complementary DNA ends (5′ RACE). Nat. Methods *2*, 629–630.

Akopian, D., Shen, K., Zhang, X., and Shan, S.O. (2013). Signal recognition particle: an essential protein-targeting machine. Annu. Rev. Biochem. *82*, 693–721.

Al-Hashimi, H.M., and Walter, N.G. (2008). RNA dynamics: it is about time. Curr. Opin. Struct. Biol. *18*, 321–329.

Altman, S., and Kirsebom, L.A. (1999). Ribonuclease P. In The RNA World, R.F. Gesteland, T. Cech, and J.F. Atkins, eds. (Cold Spring Harbor Laboratory Press), pp. 351–380.

Artsimovitch, I., and Landick, R. (2000). Pausing by bacterial RNA polymerase is mediated by mechanistically distinct classes of signals. Proc. Natl. Acad. Sci. USA *97*, 7090–7095.

Ataide, S.F., Schmitz, N., Shen, K., Ke, A., Shan, S.O., Doudna, J.A., and Ban, N. (2011). The crystal structure of the signal recognition particle in complex with its receptor. Science *331*, 881–886.

Bothwell, A.L., Garber, R.L., and Altman, S. (1976). Nucleotide sequence and in vitro processing of a precursor molecule to Escherichia coli 4.5 S RNA. J. Biol. Chem. *251*, 7709–7716.

Bustamante, C., Marko, J.F., Siggia, E.D., and Smith, S. (1994). Entropic elasticity of lambda-phage DNA. Science *265*, 1599–1600.

Chao, M.Y., Kan, M.C., and Lin-Chao, S. (1995). RNAII transcribed by IPTG-induced T7 RNA polymerase is non-functional as a replication primer for ColE1-type plasmids in Escherichia coli. Nucleic Acids Res. *23*, 1691–1695.

Chen, I., Dorr, B.M., and Liu, D.R. (2011). A general strategy for the evolution of bond-forming enzymes using yeast display. Proc. Natl. Acad. Sci. USA *108*, 11399–11404.

Chen, H., Meisburger, S.P., Pabit, S.A., Sutton, J.L., Webb, W.W., and Pollack, L. (2012). Ionic strength-dependent persistence lengths of single-stranded RNA and DNA. Proc. Natl. Acad. Sci. USA *109*, 799–804.

Chen, Y.J., Liu, P., Nielsen, A.A., Brophy, J.A., Clancy, K., Peterson, T., and Voigt, C.A. (2013). Characterization of 582 natural and synthetic terminators and quantification of their design constraints. Nat. Methods *10*, 659–664.

Chen, Y., Hu, D., Zhang, Q., Liao, X.P., Liu, Y.H., and Sun, J. (2017). Efflux pump overexpression contributes to tigecycline heteroresistance in *Salmonella enterica* serovar Typhimurium. Front. Cell. Infect. Microbiol. *7*, 37.

Comstock, M.J., Ha, T., and Chemla, Y.R. (2011). Ultrahigh-resolution optical trap with single-fluorophore sensitivity. Nat. Methods *8*, 335–340.

Dong, H., Kirsebom, L.A., and Nilsson, L. (1996). Growth rate regulation of 4.5 S RNA and M1 RNA the catalytic subunit of Escherichia coli RNase P. J. Mol. Biol. *261*, 303–308.

Doudna, J.A., and Batey, R.T. (2004). Structural insights into the signal recognition particle. Annu. Rev. Biochem. *73*, 539–557.

Frieda, K.L., and Block, S.M. (2012). Direct observation of cotranscriptional folding in an adenine riboswitch. Science *338*, 397–400.

Gabizon, R., Lee, A., Vahedian-Movahed, H., Ebright, R.H., and Bustamante, C.J. (2018). Pause sequences facilitate entry into long-lived paused states by reducing RNA polymerase transcription rates. Nat. Commun. *9*, 2930.

Gopalan, V., Baxevanis, A.D., Landsman, D., and Altman, S. (1997). Analysis of the functional role of conserved residues in the protein subunit of ribonuclease P from Escherichia coli. J. Mol. Biol. *267*, 818–829.

Gössringer, M., Helmecke, D., and Hartmann, R.K. (2012). Characterization of RNase P RNA activity. Methods Mol. Biol. *848*, 61–72.

Guo, H., Ingolia, N.T., Weissman, J.S., and Bartel, D.P. (2010). Mammalian microRNAs predominantly act to decrease target mRNA levels. Nature *466*, 835–840.

Harada, Y., Ohara, O., Takatsuki, A., Itoh, H., Shimamoto, N., and Kinosita, K., Jr. (2001). Direct observation of DNA rotation during transcription by Escherichia coli RNA polymerase. Nature *409*, 113–115.

Heilman-Miller, S.L., and Woodson, S.A. (2003). Effect of transcription on folding of the Tetrahymena ribozyme. RNA *9*, 722–733.

Hein, P.P., Palangat, M., and Landick, R. (2011). RNA transcript 3′-proximal sequence affects translocation bias of RNA polymerase. Biochemistry *50*, 7002–7014.

Hsu, L.M., Zagorski, J., and Fournier, M.J. (1984). Cloning and sequence analysis of the Escherichia coli 4.5 S RNA gene. J. Mol. Biol. *178*, 509–531.

Jagath, J.R., Matassova, N.B., de Leeuw, E., Warnecke, J.M., Lentzen, G., Rodnina, M.V., Luirink, J., and Wintermeyer, W. (2001). Important role of the tetraloop region of 4.5S RNA in SRP binding to its receptor FtsY. RNA *7*, 293–301.

Jensen, C.G., Brown, S., and Pedersen, S. (1994). Effect of 4.5S RNA depletion on Escherichia coli protein synthesis and secretion. J. Bacteriol. *176*, 2502–2506.

Keenan, R.J., Freymann, D.M., Stroud, R.M., and Walter, P. (2001). The signal recognition particle. Annu. Rev. Biochem. *70*, 755–775.

Larson, M.H., Mooney, R.A., Peters, J.M., Windgassen, T., Nayak, D., Gross, C.A., Block, S.M., Greenleaf, W.J., Landick, R., and Weissman, J.S. (2014). A pause sequence enriched at translation start sites drives transcription dynamics in vivo. Science *344*, 1042–1047.

Lewicki, B.T., Margus, T., Remme, J., and Nierhaus, K.H. (1993). Coupling of rRNA transcription and ribosomal assembly in vivo. Formation of active ribosomal subunits in Escherichia coli requires transcription of rRNA genes by host RNA polymerase which cannot be replaced by bacteriophage T7 RNA polymerase. J. Mol. Biol. *231*, 581–593.

Li, Z., Gong, X., Joshi, V.H., and Li, M. (2005). Co-evolution of tRNA 3′ trailer sequences with 3′ processing enzymes in bacteria. RNA *11*, 567–577.

Lutz, R., and Bujard, H. (1997). Independent and tight regulation of transcriptional units in Escherichia coli via the LacR/O, the TetR/O and AraC/I1-I2 regulatory elements. Nucleic Acids Res. *25*, 1203–1210.

McKinney, J., Guerrier-Takada, C., Wesolowski, D., and Altman, S. (2001). Inhibition of Escherichia coli viability by external guide sequences complementary to two essential genes. Proc. Natl. Acad. Sci. USA *98*, 6605–6610.

Moore, M.J., and Query, C.C. (2000). Joining of RNAs by splinted ligation. Methods Enzymol. *317*, 109–123.

Nechooshtan, G., Elgrably-Weiss, M., and Altuvia, S. (2014). Changes in transcriptional pausing modify the folding dynamics of the pH-responsive RNA element. Nucleic Acids Res. *42*, 622–630.

Palangat, M., Meier, T.I., Keene, R.G., and Landick, R. (1998). Transcriptional pausing at +62 of the HIV-1 nascent RNA modulates formation of the TAR RNA structure. Mol. Cell *1*, 1033–1042.

Pan, T., and Sosnick, T. (2006). RNA folding during transcription. Annu. Rev. Biophys. Biomol. Struct. *35*, 161–175.

Pan, T., Artsimovitch, I., Fang, X.W., Landick, R., and Sosnick, T.R. (1999). Folding of a large ribozyme during transcription and the effect of the elongation factor NusA. Proc. Natl. Acad. Sci. USA *96*, 9545–9550.

Peck-Miller, K.A., and Altman, S. (1991). Kinetics of the processing of the precursor to 4.5 S RNA, a naturally occurring substrate for RNase P from Escherichia coli. J. Mol. Biol. *221*, 1–5.

Perales, R., and Bentley, D. (2009). "Cotranscriptionality": the transcription elongation complex as a nexus for nuclear transactions. Mol. Cell *36*, 178–191.

Peterson, J.M., and Phillips, G.J. (2008). Characterization of conserved bases in 4.5S RNA of Escherichia coli by construction of new F′ factors. J. Bacteriol. *190*, 7709–7718.

Righini, M., Lee, A., Cañari-Chumpitaz, C., Lionberger, T., Gabizon, R., Coello, Y., Tinoco, I., Jr., and Bustamante, C. (2018). Full molecular trajectories of RNA polymerase at single base-pair resolution. Proc. Natl. Acad. Sci. USA *115*, 1286–1291.

Shen, K., Wang, Y., Hwang Fu, Y.H., Zhang, Q., Feigon, J., and Shan, S.O. (2013). Molecular mechanism of GTPase activation at the signal recognition particle (SRP) RNA distal end. J. Biol. Chem. *288*, 36385–36397.

Sinapah, S., Wu, S., Chen, Y., Pettersson, B.M., Gopalan, V., and Kirsebom, L.A. (2011). Cleavage of model substrates by archaeal RNase P: role of protein cofactors in cleavage-site selection. Nucleic Acids Res. *39*, 1105–1116.

Siu, F.Y., Spanggord, R.J., and Doudna, J.A. (2007). SRP RNA provides the physiologically essential GTPase activation function in cotranslational protein targeting. RNA *13*, 240–250.

Strobel, E.J., Watters, K.E., Nedialkov, Y., Artsimovitch, I., and Lucks, J.B. (2017). Distributed biotin-streptavidin transcription roadblocks for mapping cotranscriptional RNA folding. Nucleic Acids Res. *45*, e109.

Toulmé, F., Mosrin-Huaman, C., Sparkowski, J., Das, A., Leng, M., and Rahmouni, A.R. (2000). GreA and GreB proteins revive backtracked RNA polymerase in vivo by promoting transcript trimming. EMBO J. *19*, 6853–6859.

Tropea, J.E., Cherry, S., and Waugh, D.S. (2009). Expression and purification of soluble His(6)-tagged TEV protease. Methods Mol. Biol. *498*, 297–307.

Vioque, A., Arnez, J., and Altman, S. (1988). Protein-RNA interactions in the RNase P holoenzyme from Escherichia coli. J. Mol. Biol. *202*, 835–848.

Vvedenskaya, I.O., Vahedian-Movahed, H., Bird, J.G., Knoblauch, J.G., Goldman, S.R., Zhang, Y., Ebright, R.H., and Nickels, B.E. (2014). Interactions between RNA polymerase and the "core recognition element" counteract pausing. Science *344*, 1285–1289.

Wong, T., Sosnick, T.R., and Pan, T. (2005). Mechanistic insights on the folding of a large ribozyme during transcription. Biochemistry *44*, 7535–7542.

Wong, T.N., Sosnick, T.R., and Pan, T. (2007). Folding of noncoding RNAs during transcription facilitated by pausing-induced nonnative structures. Proc. Natl. Acad. Sci. USA *104*, 17995–18000.

Yan, S., Wen, J.D., Bustamante, C., and Tinoco, I., Jr. (2015). Ribosome excursions during mRNA translocation mediate broad branching of frameshift pathways. Cell *160*, 870–881.

Zhang, J., and Landick, R. (2016). A two-way street: regulatory interplay between RNA polymerase and nascent RNA structure. Trends Biochem. Sci. *41*, 293–310.

Zhang, D.Y., and Winfree, E. (2009). Control of DNA strand displacement kinetics using toehold exchange. J. Am. Chem. Soc. *131*, 17303–17314.

Zhao, P., Zhang, W., and Chen, S.J. (2011). Cotranscriptional folding kinetics of ribonucleic acid secondary structures. J. Chem. Phys. *135*, 245101.

STAR★METHODS

KEY RESOURCES TABLE

REAGENT or RESOURCE	SOURCE	IDENTIFIER
Antibodies		
Anti-digoxigenin (from sheep)	Sigma-Aldrich	Cat# 11333089001; RRID: AB_514496
Bacterial and Virus Strains		
DH5α competent *E. coli* cells	Thermo Fisher	Cat# 18-265-017
DH5α competent *E. coli* cells, PN25-tetR	EXPRESSYS	Cat# DH5alpha-Z1
BL21 competent *E. coli* cells, non-T7 expression	NEB	Cat# C2530H
BL21 competent *E. coli* cells, Rosetta2 (DE3) pLysS	Macrolab, QB3-Berkeley	N/A
Chemicals, Peptides, and Recombinant Proteins		
NTP set, 100 mM solution	Thermo Fisher	Cat# R0481
ApU RNA Dinucleotide (5′-3′)	TriLink	Cat# O-31004
GpC RNA Dinucleotide (5′-3′)	TriLink	Cat# O-31010
Sulfo-NHS (N-hydroxysulfosuccinimide)	Thermo Fisher	Cat# 24510
EDC (1-ethyl-3-(3-dimethylaminopropyl)carbodiimide hydrochloride)	Thermo Fisher	Cat# 77149
Heparin sodium salt	Sigma-Aldrich	Cat# H3149
Kanamycin sulfate	GoldBio	Cat# K-120-25
SYBR Green II RNA gel stain	Invitrogen	Cat# S7564
RNaseOUT	Invitrogen	Cat# 10777019
SUPERase In RNase inhibitor	Invitrogen	Cat# AM2694
Biotinylated short peptide, GGGGDGDY{K(biotin)}	Genscript	Custom order
β-casein	Sigma-Aldrich	Cat# C6905
Bovine Serum Albumin (BSA)	NEB	Cat# B900S
Streptavidin	NEB	Cat# N7021S
Turbo DNase	Invitrogen	Cat# AM2238
SuperScript IV reverse transcriptase	Invitrogen	Cat# 18090050
T4 DNA ligase	NEB	Cat# M0202L
Quick Ligation kit	NEB	Cat# M2200
Restriction enzyme, BbsI	NEB	Cat# R3539
Restriction enzyme, AvrII	NEB	Cat# R0174
Phusion® Hot Start Flex DNA polymerase	NEB	Cat# M0535S
Vent (exo-) DNA polymerase	NEB	Cat# M0257S
E. coli RNA polymerase, Holoenzyme	NEB	Cat# M0551S
Biotinylated RNA polymerase	Gabizon et al., 2018	N/A
GreB, *E. coli*	Gabizon et al., 2018	N/A
Sigma 70, *E. coli*	Gabizon et al., 2018	N/A
TEV protease	Tropea et al., 2009	N/A
Sortase	Chen et al., 2011	N/A
RNase P (M1 RNA + C5 protein), *E. coli*	Gopalan et al., 1997	N/A
Critical Commercial Assays		
Q5 site-directed mutagenesis kit	NEB	Cat# E0554
QIAquick PCR purification kit	QIAGEN	Cat# 28104
Oligonucleotides		
Lambda DNA	NEB	Cat# N3011S
bead cross-link oligo: 5′-/5AmMC6/TTAATTCATTGCGTTCTGT ACACG-3′	IDT	custom order

(*Continued on next page*)

Continued

REAGENT or RESOURCE	SOURCE	IDENTIFIER
bead cross-link complementary oligo: 5′-/5Phos/CGGTCGTGT ACAGAACGCAATGAATT-3′	IDT	custom order
gblock for mature_SRP RNA: 5′-AGTCTAACCTATAGGATACTTA CAGCCATCCCACCACAACCACCACAACCACCACAACAACA ACCAATCGGGGGCTCTGTTGGTTCTCCCGCAACGCTACTC TGTTTACCAGGTCAGGTCCGGAAGGAAGCAGCCAAGGCAG ATGACGCGTGTGCCGGGATGTAGCTGGCAGGGCCCCCAC CCCAACAAGAAACCACACAACAACACCAACAACAAACAGA CGAATTCTCATCACCATCATCCTGACTAGAG-3′	IDT	custom order
gblock for pre_SRP RNA: 5′-AGTCTAACCTATAGGATACTTACA GCCATCCCACCACAACCACCACAACCACCACAACAACAAC ACCGCGTTGGTTCTCAACGCTCTCAATGGGGGCTCTGTTG GTTCTCCCGCAACGCTACTCTGTTTACCAGGTCAGGTCCG GAAGGAAGCAGCCAAGGCAGATGACGCGTGTGCCGGGAT GTAGCTGGCAGGGCCCCCACCCCAACAAGAAACCACACAA CAACACCAACAACAAACAGACGAATTCTCATCACCATCATC CTGACTAGAG-3′	IDT	custom order
forward primer for template DNA in real-time transcription experiments: 5′-CAGATCCCGAACGCCTATC-3′	IDT	custom order
reverse primer for template DNA in real-time transcription experiments: 5′-GTCTGTTTGTTGTTGGTGTTGTTG-3′	IDT	custom order
biotinylated primer_40 bp for F-X curve measurements: 5′-/5Biosg/GTAAACAGAGTAGCGTTGCG-3′	IDT	custom order
biotinylated primer_52 bp for F-X curve measurements: 5′-/5Biosg/GGACCTGACCTGGTAAACAG-3′	IDT	custom order
biotinylated primer_84 bp for F-X curve measurements: 5′-/5Biosg/ACACGCGTCATCTGCC-3′	IDT	custom order
biotinylated primer_97 bp for F-X curve measurements: 5′-/5Biosg/GCTACATCCCGGCACAC-3′	IDT	custom order
biotinylated primer_114+16 bp for F-X curve measurements: 5′-/5Biosg/GTGTGGTTTCTTGTTGGGGTG-3′	IDT	custom order
biotinylated primer_114+39 bp for F-X curve measurements: 5′-/5Biosg/GTCTGTTTGTTGTTGGTGTTGTTG-3′	IDT	custom order
antisense oligo-1: 5′-CAGAGCCCCC-3′	IDT	custom order
antisense oligo-2: 5′-GACCTGACCTGG-3′	IDT	custom order
gblock for T7A1_4.5S RNA: 5′-GGAAACAGCTATGACCATGATTA CGCCAAGCTTAAAAGATTAATTTAAAATTTATCAAAAAGAGTA TTGACTTAAAGTCTAACCTATAGGATACTTACAGCCGCGTTG GTTCTCAACGCTCTCAATGGGGGCTCTGTTGGTTCTCCCGC AACGCTACTCTGTTTACCAGGTCAGGTCCGGAAGGAAGCA GCCAAGGCAGATGACGCGTGTGCCGGGATGTAGCTGGCA GGGCCCCCACCCATTTCTGCCTCCCACCGTTTCGTCAAAAA ATCCCAACATGGCTAAACT-3′	IDT	custom order
common forward primer for stalling template DNA: 5′-GGAAACAGCTATGACCATGATTACGCC-3′	IDT	custom order
biotinylated reverse primer-1 for stalling template DNA (24+22): 5′-CCGGACC/iBiodT/GACCTGGTAAACAG-3′	IDT	custom order
biotinylated reverse primer-2 for stalling template DNA (24+30): 5′-GCTTCCT/iBiodT/CCGGACCTGACC-3′	IDT	custom order
biotinylated reverse primer-3 for stalling template DNA (24+66): 5′-CTACA/iBiodT/CCCGGCACACGC-3′	IDT	custom order
biotinylated reverse primer-4 for stalling template DNA (24+114): 5′-CCATGTTGGGATTTTT/iBiodT/GACGAA ACGGTG-3′	IDT	custom order

(*Continued on next page*)

Continued

REAGENT or RESOURCE	SOURCE	IDENTIFIER
cDNA primer for reverse transcription: 5′-/5TYE665/ GTAAACAGAGTAGCGTTGCGGGAG-3′	IDT	custom order
gblock for pZE21_4.5S_rrnC: 5′-CACGAGGCCCTTTCGTCTTCAC TCCCTATCAGTGATAGAGATTGACATCCCTATCAGTGATAGAG ATACTGAGCACGCGTTGGTTCTCAACGCTCTCAATGGGGGCT CTGTTGGTTCTCCCGCAACGCTACTCTGTTTACCAGGTCAGG TCCGGAAGGAAGCAGCCAAGGCAGATGACGCGTGTGCCGG GATGTAGCTGGCAGGGCCCCCACCCCAGATAAAAAAAATCC TTAGCTTTCGCTAAGGATGATTTCTACCTAGGGCGTTC-3′	IDT	custom order
Recombinant DNA		
pZ vector (pZE21MCS)	EXPRESSYS	Cat# pZE21MCS
pZE21_wtSRP_FL_rrnC	This paper	N/A
pZE21_SRP_100_rrnC	This paper	N/A
pZE21_U18C_FL_rrnC	This paper	N/A
pZE21_U18C_100_rrnC	This paper	N/A
pZE21_U3234C_FL_rrnC	This paper	N/A
pZE21_U3234C_100_rrnC	This paper	N/A
PGMZ plasmid	This paper	N/A
pIA1127	This paper	N/A
pIA1234	This paper	N/A
Software and Algorithms		
LabVIEW	National Instruments	N/A
MATLAB	Mathworks	N/A
Igor Pro	WaveMetrics	N/A
Other		
Mono Q 5/50 GL, anion exchange chromatography column	GE Healthcare	Cat# 17-5166-01
HiPrep 16/60 Sephacryl S-300 HR Column	GE Healthcare	Cat# 17-1167-01
Carboxylated polystyrene beads, 1-μm	Bang Laboratories	Cat# PC04N
Streptavidin coated polystyrene beads, 0.82-μm	Spherotech	Cat# SVP-08-10

LEAD CONTACT AND MATERIALS AVAILABILITY

Further information and requests for resources should be directed to and will be fulfilled by the Lead Contact, Carlos Bustamante (carlosb@berkeley.edu).

METHOD DETAILS

Optical Tweezers

A home-built optical tweezers instrument was assembled as described previously (Gabizon et al., 2018; Righini et al., 2018). Briefly, an Nd:YAG 1,064-nm laser was used. The two traps were generated by switching a single beam at high rate using acoustic-optic deflector (AOD). The frequency of the AOD was controlled by a custom-made radio frequency board (Comstock et al., 2011), and the position of the traps were switched every 5 μs. In this case, detection of the bead positions in both traps was achieved on the same quadrant photodiode (QPD).

SRP RNA Encoded Template DNA

A DNA fragment (IDT) coding for the *Escherichia coli* (*E. coli*) SRP RNA (138-bp for pre-SRP RNA, or 114-bp for mature SRP RNA) was first cloned into a PGMZ plasmid at 42-bp downstream of T7A1 promoter. Specific length of template DNAs—either full-length for real-time transcription experiments or truncated versions for nascent RNA folding intermediate unfolding assessments—was then amplified by PCR (using different reverse primers, IDT) from the cloned plasmid. The short G-less sequence placed downstream of the T7A1 promoter allows us to stall the RNAP transcription right before the beginning of SRP RNA, which we will then restart on the optical tweezers setup by supplementing the full set of NTPs (see main text). Also, it is with this stretch of initially transcribed stalled sequence on the nascent RNA 5′ end that a 5′ overhang bearing dsDNA handle anneals so as to catch the RNA tether on the

optical tweezers. To prepare DNA templates for truncated SRP RNA folding intermediates stalled on the RNAP surface (Figure S3), the corresponding PCR reactions were performed with biotinylated reverse primers (IDT).

DNA Handle

The DNA handles were prepared by PCR using lambda DNA as the template, and with biotinylated or digoxigenin-labeled oligonucleotides (IDT) as primers (right- and left-hand side of the DNA handles shown in Figure 2A), purified following standard protocol from PCR purification kit (QIAGEN). To create the DNA handle bearing a 5′ overhang complementary to the nascent RNA 5′ end, a 1', 2′-Dideoxyribose was introduced in the DNA primer (IDT) and used in the PCR reaction.

Bead Surface Functionalization

Anti-digoxigenin (AD) antibody coated beads

50 μL of 5% (w/v) 1-μm diameter carboxylated polystyrene beads (Spherotech) were washed with 1 mL activation buffer (100 mM MES-NaOH, pH 6, 500 mM NaCl) three times, with centrifugation steps (3 min at 3000 rpm) between wash steps. EDC and sulfo-NHS (Thermo Scientific) were then added to the bead solution to final concentration of ∼5 mM and ∼10 mM, respectively. After incubation for 15 min at room temperature, the reaction was quenched by adding 2.8 μL 2-mercaptoethanol (40 mM). After washing the beads with activation buffer, the anti-digoxigenin antibody was incubated with bead solution by tumbling at room temperature.

The reaction proceeded for 2 hours. The beads were washed with quenching buffer (100 mM Tris-HCl pH 7) and storage buffer (40 mM HEPES-KOH, pH 7.5, 100 mM KCl), and stored at 4°C.

Oligo coated beads

To prepare a double stranded oligo for bead surface coupling reaction, 5′ end amino modified DNA oligo (5′-/5AmMC6/TTAATT CATTGCGTTCTGTACACG-3′, IDT) was hybridized to a 5′-phosporylated DNA oligo (5′-/5Phos/CGGTCGTGTACAGAACGCAAT GAATT-3′, IDT). Annealing was performed by heating the mixture of DNA oligo (0.25 mM each) to 95°C for 10 min, followed by cooling to room temperature. 10 μL of 10% (w/v) 1 μm-diameter carboxylated polystyrene beads (Spherotech) were washed four times with coupling buffer (100 mM MES-NaOH pH 4.7, 150 mM NaCl, 5% DMSO), and spun down (5 min at 4500 g) between washes. The annealed double stranded oligo and EDC (Thermo Scientific Pierce) were then added to the washed beads to a final concentration of ∼1.5 μM and ∼300 mM, respectively. After incubation for 2 hours with vigorous shaking, more EDC (final concentration ∼500 mM) was added, followed by overnight shaking at room temperature. The reaction was quenched upon the addition of glycine (final concentration ∼50 mM). Lastly the bead solution was washed with stock buffer (20 mM Tris-HCl, pH 8, 1 mM EDTA, 0.05% Tween 20, 5 mM NaN_3) four times and stored at 4°C.

Beads passivation

The above functionalized beads (1%, w/v) were passivated by diluting 10-fold in TE buffer (20 mM Tris-HCl, pH 8, 1 mM EDTA) and addition of casein to a final concentration of 1 mg/ml. Then the bead sample was incubated with vortex for ∼1 hour at room temperature and washed with TE buffer by centrifugation (3 min at 4500 g), and stored at 4°C. 0.82-μm diameter streptavidin coated beads (Spherotech) were also passivated following the same protocol.

Recombinant Proteins

Preparation of sigma 70

Plasmid pIA1127 was transformed into Rosetta2 bacteria. The bacteria were grown in 2 L of 2YT medium supplemented with 1% glucose, NPS (25 mM $(NH_4)_2SO_4$, 50 mM KH_2PO_4, 50 mM Na_2HPO_4), 1 mM magnesium sulfate, 34 μg/ml chloramphenicol, and 50 μg/ml kanamycin. The culture was grown at 37°C and transferred to 17°C. Then IPTG was added to 0.1 mM and incubated for 16 hours. For purification, the bacteria were dispersed in 80 mL of buffer A25 (20 mM Tris-HCl, pH 7.5, 0.5 M NaCl, 10% glycerol, 25 mM imidazole, 2 mM beta-mercaptoethanol) supplemented with 0.1 mg/ml lyzozyme and protease inhibitors (Roche). The bacteria were then lysed via French press, and the lysate was clarified by centrifugation and filtration and loaded onto a 5 mL Ni-NTA column. The column was washed with 20 mL buffer A25 and 20 mL buffer A50 (A25 + 50 mM imidazole), and the his-tagged sigma 70 was eluted in buffer A300 (A25 + 300 mM imidazole). For the removal of the his-tag on sigma 70, TEV protease (Tropea et al., 2009) was added to the eluted protein at a molar ratio of 1:40, and reacted overnight at 4°C while being dialyzed against A50. The protein was then again passed through a Ni-NTA column. The flow-through, containing non–his-tagged sigma 70 was collected, concentrated and purified by gel filtration on a sephacryl S300 column equilibrated with buffer B (20 mM Tris, pH 7.5, 0.5 M NaCl, 10% glycerol, 1 mM EDTA, 1 mM DTT). Aliquots were flash-frozen in liquid nitrogen and stored at −80°C.

To form the holoenzyme, the sample was incubated with a twofold excess of purified sigma 70 overnight on ice and diluted 10-fold with buffer B0 (50 mM Tris-HCl, pH 6.9, 5% glycerol, 0.5 mM EDTA, 1 mM DTT) and loaded on a heparin 5 mL column. A gradient of 50 mM to 1 M NaCl was used to elute the protein. RNAP holoenzyme was separated clearly from excess sigma 70. The sample was dialyzed against buffer B50 (50 mM Tris-HCl, pH 6.9, 5% glycerol, 50 mM NaCl, 0.5 mM EDTA, 1 mM DTT) and then purified further on a 1 mL monoQ column using a 50 mM to 1 M NaCl gradient (again, the sample was split into three portions loaded separately). Pure fractions were pooled, dialyzed against storage buffer (20 mM Tris-HCl, pH 7.5, 200 mM KCl, 0.2 mM EDTA, 0.2 mM DTT, 5% glycerol), aliquoted, flash-frozen, and stored at −80°C.

Preparation of sortagged RNA polymerase holoenzyme

Plasmid pIA1234 was transformed into Rosetta2 bacteria. Sortag-RNAP was expressed using the same protocol as sigma 70, except that ampicillin was used instead of kanamycin. For purification, the cells were dispersed in 75 mL of lysis buffer (50 mM Tris-HCl, pH 6.9, 0.5 M NaCl, 5% glycerol) supplemented by 0.1 mg/ml lyzozyme and protease inhibitors and lysed via French press. The lysate was centrifuged and filtered, and imidazole was added to 20 mM. The protein was loaded onto a 5 mL Ni-NTA column. The column was washed with 30 mL of lysis buffer plus 20 mM imidazole, and the his-tagged RNAP core enzyme was eluted in lysis buffer plus 250 mM imidazole. To form the holoenzyme, the sample was incubated with a twofold excess of purified sigma 70 overnight on ice and diluted 10-fold with buffer B0 (50 mM Tris-HCl, pH 6.9, 5% glycerol, 0.5 mM EDTA, 1 mM DTT) and loaded onto a heparin 5 mL column. A gradient of 50 mM to 1 M NaCl was used to elute the protein. RNAP holoenzyme was separated clearly from excess sigma 70. The sample was dialyzed against buffer B50 (50 mM Tris-HCl, pH 6.9, 5% glycerol, 50 mM NaCl, 0.5 mM EDTA, 1 mM DTT) and then purified further on a 1 mL monoQ column using a 50 mM to 1 M NaCl gradient (again, the sample was split into three portions loaded separately). Pure fractions were pooled, dialyzed against storage buffer (20 mM Tris-HCl, pH 7.5, 200 mM KCl, 0.2 mM EDTA, 0.2 mM DTT, 5% glycerol), aliquoted, flash-frozen, and stored at −80°C.

Biotinylation of sortag-RNA polymerase

We obtained a peptide containing an N-terminal GGG tag with a biotin-modified lysine residue (Genscript): GGGGDGDY{K(biotin)}. We reacted 100 μL of 9.6 μM sortag-RNAP with a 200-fold excess of biotinylated peptide in 200 μL coupling buffer (50 mM Tris-HCl, pH 7.5, 5 mM $CaCl_2$) containing 2 μM sortase (Chen et al., 2011). The reaction proceeded for 60 min. At this point, imidazole was added to 25 mM and NaCl to 350 mM, and the sample was passed through 70 μL Ni-NTA beads to remove sortase and unreacted RNAP. The excess peptide was removed by dialysis into storage buffer, and the biotinylated RNAP was stored in storage buffer at −80°C.

Preparation of GreB

GreB was purified as described previously (Gabizon et al., 2018).

Real-Time Co-transcriptionalFolding of Nascent RNA

Stalled RNAP-RNA complexes were prepared by incubating biotinylated RNAPs with template DNAs in TB20 buffer (20 mM Tris-HCl, pH 8, 20 mM NaCl, 10 mM $MgCl_2$, 20 mM DTT, 1 mg/ml BSA) containing 5 μM ATP, CTP, 150 μM ApU and RNaseOut (ThermoFisher) for 20 minutes at 37°C. Stalled complexes were then incubated for another 20 min together with heparin and digoxigenin-labeled 1.5-kbp DNA handle bearing a 5′ overhang complementary to the 5′ stretch of nascent RNA transcripts. 1-μm diameter anti-digoxigenin coated (AD) beads were then added to the stalled complexes. After 20 min incubation, the mixture was diluted into 1 mL TB130 buffer (20 mM Tris-HCl, pH 8, 130 mM KCl, 10 mM $MgCl_2$, 0.1 mM EDTA, 0.1 mM DTT and 10 mM NaN_3). Meanwhile, 1-μm diameter oligo-coated beads were ligated to the 5′ overhang of another 1.5-kbp DNA handle which is biotin-labeled on its other end (Figure 2A); the ligation reaction is carried out in TB20 buffer including 0.4 units of T4 DNA ligase and 0.1 mM ATP for 1 hour at room temperature. Following the ligation, the handle-bead mixture was incubated with streptavidin for another 20 min and finally diluted into 1 mL TB130 buffer. Next the stalled complex bead and handle-bead samples were delivered into the microfluidic chamber on the optical tweezers setup and trapped by the two laser beams, respectively. The two beads were then brought to close proximity of each other, such that a tether could form between the streptavidin bound on the 1.5-kbp DNA handle and the biotin labeled on the RNAP (Figure 2A). Once a stalled RNAP:RNA complex is tethered on the optical tweezers setup, the synthesis of nascent transcript is fueled by flowing TB130 buffer containing NTPs into the chamber, where the extension/growth of the RNA is monitored under constant force. For real-time transcription experiments conducted in the presence of GreB or antisense oligo, the transcription buffer was further supplemented with 1 μM of GreB, or 10 μM HPLC-purified antisense oligo (IDT).

Force-Extension (F-X) Curve Measurements of Truncated and Full-Length SRP RNA on the Surface of RNA Polymerase

As a roadblock to stall RNAP on the template DNAs of different length—so as to transcribe specific length of nascent SRP RNA transcript (Figure S3), a streptavidin was bound to the biotin labeled at the downstream end of the template DNA; the mixture is incubated in TB20 buffer at room temperature for 1 hour. Stalled complexes were then prepared by incubating DNA:streptavidin complex with RNAP in TB20 buffer containing 5 μM ATP, CTP, 150 μM ApU and RNaseOut (ThermoFisher) for 20 minutes at 37°C. Stalled complexes were then incubated for another 20 min together with heparin and digoxigenin-labeled 1.5-kbp DNA handle bearing a 5′ overhang complementary to the 5′ stretch of nascent RNA transcripts. 1-μm diameter anti-digoxigenin coated (AD) beads were then added to the stalled complexes; all procedures up till now are the same as those in the above real-time stalled complex preparation. After 20 min incubation, the mixture was incubated with NTPs (~50 μM) for 1 min to further transcribe SRP RNA from the template DNA, and finally diluted into 1 mL TB130 buffer. Meanwhile, the handle-bead sample was prepared following the same ligation protocol as that used in the real-time transcription experiments, but diluted into TB130 buffer without further incubation with streptavidin. In this case, a stalled RNAP:RNA complex is tethered on the optical tweezers setup via the binding interaction between the streptavidin at the downstream end of template DNA and the biotin labeled on the 1.5-kbp DNA handle.

Force-Extension (F-X) Curve Measurements of Truncated and Full-Length SRP RNA in Isolation

A purified SRP RNA was incubated with digoxigenin-labeled 1.5-kbp DNA handle bearing a 5′ overhang complementary to the 5′ stretch of RNA in TB20 buffer for 20 minutes. 1-μm diameter anti-digoxigenin antibody coated (AD) beads were then added to RNA-handle complexes. After 20 min incubation, the mixture was diluted into TB130 buffer. For the other side of the tethering beads, 0.82-μm diameter streptavidin coated beads were incubated with a biotin-labeled 1.5-kbp DNA handle bearing a 3′ overhang (Yan et al., 2015) complementary to the 3′ stretch of RNA in TB20 buffer for 20 min, and the mixture was diluted in TB130 buffer. Tethering between the 1-μm and 0.82-μm beads trapped on the optical tweezers setup was made via the complementary sequences of RNA 3′ stretch and the biotin-labeled DNA handle 3′ overhang.

Unit Conversion of Transcription Trajectories Recorded in Nanometers into Nucleotides

In order to convert the observed transcription extension recorded in nanometers into nucleotides, we consider the force-dependent characteristics determined from the extensible worm-like chain (WLC) model (Bustamante et al., 1994):

$$\frac{FP}{k_BT} = \frac{1}{4}\left(1 - \frac{x}{L}\right)^{-2} - \frac{1}{4} + \frac{x}{L} - \frac{F}{K} \qquad \text{(Equation 1)}$$

where k_B is the Boltzmann constant, K is the elastic modulus, L is the counter length, and P is the persistence length, which represents the stiffness of RNA and greatly impacts the conversion factor between nanometers and nucleotides. It has been shown that persistence length is altered by buffer conditions such as ionic strength (Chen et al., 2012), where changes in [NTP] under fixed [Mg^{2+}] affect the RNA extension change observed at the same constant force on the optical tweezers. To determine the persistence length in our experimental conditions, we measure the unfolding/refolding extension change in nanometer of a known RNA hairpin which is 180-bp long (Yan et al., 2015), and calculate the conversion factors (nt/nm) under specific constant force applied and at a given [NTP] (see Table S1). These empirically determined values were also verified using the full-length SRP RNA (in the absence of RNAP), which readily adopts its 50-bp long native hairpin fold.

RNase P Processing Assay

Four stalled RNAP-RNA complexes (see main text) were prepared using the aforementioned streptavidin roadblock method to stall RNAP on a biotinylated template DNA, where the biotin is located ~10-nt downstream of the desired stalled site and is on the template strand to achieve high stalling efficiency (Strobel et al., 2017). Specifically, 4.5 pmole of biotinylated DNA template (PCR products using Vent (exo-) DNA polymerase from NEB, and primers with internal biotin modifications from IDT; gel-purified) was pre-incubated with 225 pmole streptavidin (NEB) at room temperature for 30 min (total volume 18.75 μl; in 1x *E. coli* RNA polymerase reaction buffer; M0551, NEB). Meanwhile, 1.5 μL of 3 μM C5 protein is pre-incubated at 37°C for 5 min, and then incubated with 1.5 μL of 0.6 μM M1 RNA for another 10 min at 37°C to form the RNase P complex (gift from Dr. Lien Lai and Prof. Venkat Gopalan) (Gopalan et al., 1997; Gössringer et al., 2012; Vioque et al., 1988). Next, 16.5 μL reaction mixtures containing 9.375 μL DNA-roadblock template (final 136 nM), 1.5 μL RNase P complex (final 27 nM; or 1.5 μL 1x buffer for control), and 5.625 μL of RNAP solution (final: 0.20U/μl RNAP; M0551, NEB; 0.45 mM NTP; 0.04 mM GpC, TriLink; 0.3U/μl SUPERase•In, Invitrogen; 1x reaction buffer) were incubated at 37°C for 10 min. 1.1 μL of Turbo DNase (Ambion) is then added to the above reaction to digest away the DNA template (37°C for 15 min). 8 μL of the above final mixtures were quenched with equal volume of gel loading buffer (final 49.5% formamide, 9 mM EDTA; Ambion) and loaded onto Urea PAGE gel (7M, 12%, Figure 4B) to visualize the RNA products. The other 8 μL is mixed with 1 μL glycogen (0.5 mg/ml) prior to phenol/chloroform extraction and ethanol precipitation, so as to concentrate the RNA products for reverse transcription of cDNA with a 5′-TYE665-labeled DNA oligo primer (IDT) using SuperScript IV (Invitrogen). Half of the above reaction is loaded onto Urea PAGE gel to visualize the cDNA products (in the red fluorescence channel; Figure 4C) as well as the RNAs (SYBR Green II staining). The other half of the cDNA products, after phenol/chloroform extraction and ethanol precipitation, is ligated (T4 DNA ligase; M0202, NEB) to a donor DNA oligo for PCR amplification (Phusion DNA polymerase; M0535, NEB) (Nat. Methods, 2005; Guo et al., 2010; Moore and Query, 2000). The resultant DNA products were then gel-purified, where individual bands were eluted separately and sent for sequencing (Sequetech).

Plasmid Constructs for Cell Viability Experiments

pZE21MCS (MCS: multiple cloning sites; sold by Expressys; a gift from A. Flamholz) and customized gblocks (~500 bp long double-stranded DNAs, which sequence from 5′ to 3′ contains: $P_{LtetO-1}$ promoter, specific SRP RNA variant sequence, rrnC terminator, and a second $P_{LtetO-1}$; purchased from IDT) were digested with BbsI and AvrII (R3539 and R0174, NEB), ligated with quick T4 ligase kit (M2200, NEB) following NEB protocol, and transformed into an *E. coli* cloning strain, DH5alpha-Z1 (Expressys). A series of plasmids (pZE21_SRP_rrnC) were constructed: pZE21_wtSRP_FL_rrnC, pZE21_SRP_100_rrnC, pZE21_U18C_100_rrnC, pZE21_U3234C_100_rrnC, pZE21_empty_rrnC, and pZE21_SRP_100_rrnC_read-through. The plasmids harboring full-length SRP RNA sequence mutants (U18C and U32C/U34C) were prepared from pZE21_wtSRP_FL_rrnC using the Q5 site-directed mutagenesis kit (E0554, NEB), and following protocols therein for appropriate primer designs and sequential procedures to obtain the modified plasmids (pZE21_U18C_FL_rrnC and pZE21_U3234C_FL_rrnC).

Since the 24-nt long 5′-precursor sequence in the pre-SRP RNA (i.e., 4.5S RNA) does not interfere with the co-transcriptional folding of SRP RNA (see main text), it is not included in these plasmid constructs prepared for our cell viability experiment. Leaving

out the 5′-precursor also eliminates the possibility that the maturation, instead of the proper folding, of SRP RNA is the cause for any changes seen with cell viability. This potential complication is due to the fact that RNase P—the processing enzyme that cleaves off the 5′-precursor from SRP RNA—is five times less abundant than the endogenous pre-SRP RNA (Dong et al., 1996), and would be even more limiting if it were to process an exceeding amount of exogenous pre-SRP RNA variants that are highly transcribed inside the transformed cells. Furthermore, RNase P also processes many other essential functional RNAs such as tRNAs. In other words, any shortage (or sequestering) of this processing enzyme will inevitably impact the overall cell viability and compromise the interpretation of our analysis. Therefore, to better and directly correlate how the folding of SRP RNA influences its functionality and ultimately the cell viability, we choose to not include its 5′-precursor in the plasmid constructs prepared for our *in vivo* studies.

The fact that the same promoter sequence (i.e., $P_{LtetO-1}$) is used to regulate the transcription of desired RNA products, and that the cloning plasmid is of high copy number (i.e., colE1 replication origin; 70-100 plasmid copy number/cell), ensures similar overexpression levels of the SRP RNA variants examined in the cell experiments. We have verified that similar amounts of plasmid are indeed maintained in the bacteria. Specifically, at each round of cell growth experiment, we isolated the plasmids from transformed cells (of the same cell density [OD_{600}] and culture volume) to confirm the yield of the plasmids as well as the propagation of the correct sequence for each SRP RNA variant. To verify the same promoter indeed behaves the same for different variants inserted downstream in the plasmid, we have also performed *in vitro* transcription with the isolated plasmids and found similar yields in the RNA products transcribed (data not shown). Based on the above information and characterizations, we can attribute the observed impacts on the cell viability—not to the differences in expression levels but—to the changes in RNA folding of different SRP RNA variants examined.

CompletePlasmid Sequence of pZE21_wtSRP_FL_rrnC

Please see the last two pages in the Supplemental Data file for detailed notations on the sequence elements and specific features highlighted within the plasmid.

5′-CTAGGCGTTCGGCTGCGGCGAGCGGTATCAGCTCACTCAAAGGCGGTAATACGGTTATCCACAGAATCAGGGGATAACGCAG
GAAAGAACATGTGAGCAAAAGGCCAGCAAAAGGCCAGGAACCGTAAAAAGGCCGCGTTGCTGGCGTTTTTCCATAGGCTCCGC
CCCCCTGACGAGCATCACAAAAATCGACGCTCAAGTCAGAGGTGGCGAAACCCGACAGGACTATAAAGATACCAGGCGTTTCC
CCCTGGAAGCTCCCTCGTGCGCTCTCCTGTTCCGACCCTGCCGCTTACCGGATACCTGTCCGCCTTTCTCCCTTCGGGAAGCGT
GGCGCTTTCTCAATGCTCACGCTGTAGGTATCTCAGTTCGGTGTAGGTCGTTCGCTCCAAGCTGGGCTGTGTGCACGAACCCCCC
GTTCAGCCCGACCGCTGCGCCTTATCCGGTAACTATCGTCTTGAGTCCAACCCGGTAAGACACGACTTATCGCCACTGGCAGCA
GCCACTGGTAACAGGATTAGCAGAGCGAGGTATGTAGGCGGTGCTACAGAGTTCTTGAAGTGGTGGCCTAACTACGGCTACAC
TAGAAGGACAGTATTTGGTATCTGCGCTCTGCTGAAGCCAGTTACCTTCGGAAAAAGAGTTGGTAGCTCTTGATCCGGCAAACAA
ACCACCGCTGGTAGCGGTGGTTTTTTTGTTTGCAAGCAGCAGATTACGCGCAGAAAAAAAGGATCTCAAGAAGATCCTTTGATCTT
TTCTACGGGGTCTGACGCTCAGTGGAACGAAAACTCACGTTAAGGGATTTTGGTCATGACTAGTGCTTGGATTCTCACCAATAAAA
AACGCCCGGCGGCAACCGAGCGTTCTGAACAAATCCAGATGGAGTTCTGAGGTCATTACTGGATCTATCAACAGGAGTCCAAGC
GAGCTCTCGAACCCCAGAGTCCCGCTCAGAAGAACTCGTCAAGAAGGCGATAGAAGGCGATGCGCTGCGAATCGGGAGCGGC
GATACCGTAAAGCACGAGGAAGCGGTCAGCCCATTCGCCGCCAAGCTCTTCAGCAATATCACGGGTAGCCAACGCTATGTCCT
GATAGCGGTCCGCCACACCCAGCCGGCCACAGTCGATGAATCCAGAAAAGCGGCCATTTTCCACCATGATATTCGGCAAGCAGG
CATCGCCATGGGTCACGACGAGATCCTCGCCGTCGGGCATGCGCGCCTTGAGCCTGGCGAACAGTTCGGCTGGCGCGAGCCC
CTGATGCTCTTCGTCCAGATCATCCTGATCGACAAGACCGGCTTCCATCCGAGTACGTGCTCGCTCGATGCGATGTTTCGCTTG
GTGGTCGAATGGGCAGGTAGCCGGATCAAGCGTATGCAGCCGCCGCATTGCATCAGCCATGATGGATACTTTCTCGGCAGGAG
CAAGGTGAGATGACAGGAGATCCTGCCCCGGCACTTCGCCCAATAGCAGCCAGTCCCTTCCCGCTTCAGTGACAACGTCGAG
CACAGCTGCGCAAGGAACGCCCGTCGTGGCCAGCCACGATAGCCGCGCTGCCTCGTCCTGCAGTTCATTCAGGGCACCGGAC
AGGTCGGTCTTGACAAAAAGAACCGGGCGCCCCTGCGCTGACAGCCGGAACACGGCGGCATCAGAGCAGCCGATTGTCTGTTG
TGCCCAGTCATAGCCGAATAGCCTCTCCACCCAAGCGGCCGGAGAACCTGCGTGCAATCCATCTTGTTCAATCATGCGAAACGA
TCCTCATCCTGTCTCTTGATCAGATCTTGATCCCCTGCGCCATCAGATCCTTGGCGGCAAGAAAGCCATCCAGTTTACTTTGCAGG
GCTTCCCAACCTTACCAGAGGGCGCCCCAGCTGGCAATTCCGACGTCTAAGAAACCATTATTATCATGACATTAACCTATAAAAA
TAGGCGTATCACGAGGCCCTTTCGTCTTCACCTCGAGTCCCTATCAGTGATAGAGATTGACATCCCTATCAGTGATAGAGATACT
GAGCACATCGGGGGCTCTGTTGGTTCTCCCGCAACGCTACTCTGTTTACCAGGTCAGGTCCGGAAGGAAGCAGCCAAGGCAG
ATGACGCGTGTGCCGGGATGTAGCTGGCAGGGCCCCCACCCCAGATAAAAAAAATCCTTAGCTTTCGCTAAGGATGATTTCTCC
TCGAGGTCGACGGTATCGATAAGCTTGATATCGAATTCCTGCAGCGGATCCCATGGAGGCATTCCCTATCAGTGATAGAGATTGA
CATCCCTATCAGTGATAGAGATACTGAGCACATCTTGCCATGTGTATGTGGGAGACGGTCGGGTCCAGATATTCGTATCTGTCGA
GTAGAGTGTGGGCTCCCACATACTCTGATGATCCTTCGGGATCATTCATGGCAATCTAGACAGATAAAAAAAATCCTTAGCTTTCG
CTAAGGATGATTTCTAC-3′

Cell Viability Plate Assay

BL21 (non-T7 expression, C2530H from NEB) were transformed with purified, sequencing-verified plasmids (pZE21_SRP_rrnC) that carry specific SRP RNA variants (following protocol from NEB; 50 ng plasmid per 50 μL competent cell) and plated on kanamycin (40 μg/ml) LB agar plates. Images of the plates, showing the emergence of colonies that carry plasmids encoding with specific

SRP RNA variants, were taken after 12-16 hours of growth at 37°C. At least 5 colonies were picked from each transformation experiments and sent for sequencing (Sequetech) to confirm the plasmid constructs therein.

Recovery/Post-Relaxation Growth Rate

BL21 (non-T7 expression, C2530H from NEB) were transformed with purified, sequencing-verified plasmids (pZE21_SRP_rrnC) that carry specific SRP RNA variants (following protocol from NEB; 50 ng plasmid per 50 μL competent cell) and plated on kanamycin (40 μg/ml) LB agar plates. A single colony was picked and inoculated into 10 ml of LB (antibiotic-free), and let grow at 37°C with shaking at 180 rpm for 6 hours. We then split each culture sample in half, where 5 mL continues to grow in LB (i.e., permissive condition), and the other 5 mL grows in the presence of kanamycin (final conc. 40 μg/ml), for another 10 hours. After a total of 16 hours (6+10) overnight growth, aliquot from each culture is diluted with LB plus kanamycin (final conc. 40 μg/ml) to OD600 = 0.02 as the starting point of recovery growth (t_0). We then record OD600 every 30-45 min interval, to monitor the rate of growth at 37°C, for a total of 3-4 hours until the culture reaches the mid-log phase (OD600 = 0.6-0.8).

QUANTIFICATION AND STATISTICAL ANALYSIS

Statistical details of individual experiments, including numbers of observations, numbers of replicates, and dispersion and precision measures, are as described in the manuscript text, figure legends, and the figures themselves.

DATA AND CODE AVAILABILITY

The full dataset will be made available upon request.

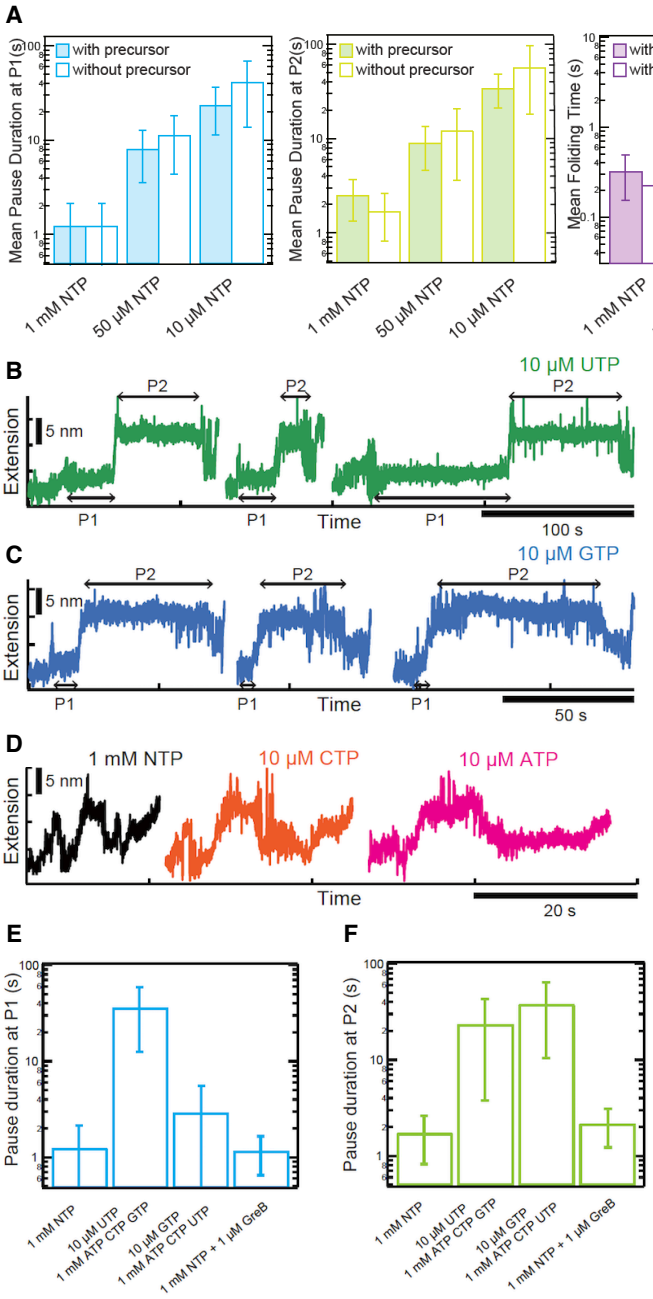
A
Mean Pause Duration at P1(s)
with precursor
without precursor
1 mM NTP
50 µM NTP
10 µM NTP
Mean Pause Duration at P2(s)
Mean Folding Time (s)
B
10 µM UTP
Extension
5 nm
P2
P1
Time
100 s
C
10 µM GTP
50 s
D
1 mM NTP
10 µM CTP
10 µM ATP
20 s
E
Pause duration at P1 (s)
10 µM UTP
1 mM ATP CTP GTP
10 µM GTP
1 mM ATP CTP UTP
1 mM NTP + 1 µM GreB
F
Pause duration at P2 (s)

Figure S1

Figure S1. Characterizing the Mean Durations of Transcription Pauses and Mean Time Span After Pause in the SRP RNA Co-transcriptional Folding Trajectories: as a Function of [NTP], of the Presence and Absence of the Precursor Sequence, and of Specific Nucleotide Depletion; Related to Figure 2

(A) Mean durations for P1 pause (left), mean durations for P2 pause (middle), and mean time span after P2 pause (right; corresponding to purple regions in Figure 2B) in the SRP RNA co-transcriptional folding trajectories, which were recorded in the presence and absence of the 5'-precursor sequence (filled and empty bars, respectively), and at three NTP concentrations: 1 mM (n=14, 11), 50 μM (n=14, 14), and 10 μM (n=13, 12).

(B) Representative traces of SRP RNA co-transcriptional folding at [UTP] = 10 μM (1 mM each for ATP, CTP, and GTP). Both P1 and P2 pauses are prolonged.

(C) Representative traces of SRP RNA co-transcriptional folding at [GTP] = 10 μM (1 mM each for ATP, CTP, and UTP). Only P2 pause duration is prolonged.

(D) Representative traces of SRP RNA co-transcriptional folding at low [CTP] (orange) or low [ATP] (magenta) ([CTP] or [ATP] = 10 μM, while the others are at 1 mM). The trace at saturating [NTP] (1 mM each; black) is shown for comparison.

(E-F) Mean durations for P1 and P2 pauses at saturating [NTP] (n=11), low [UTP] (n=10), low [GTP] (n=12) transcription conditions, and in the presence of 1 μM GreB (n=10).

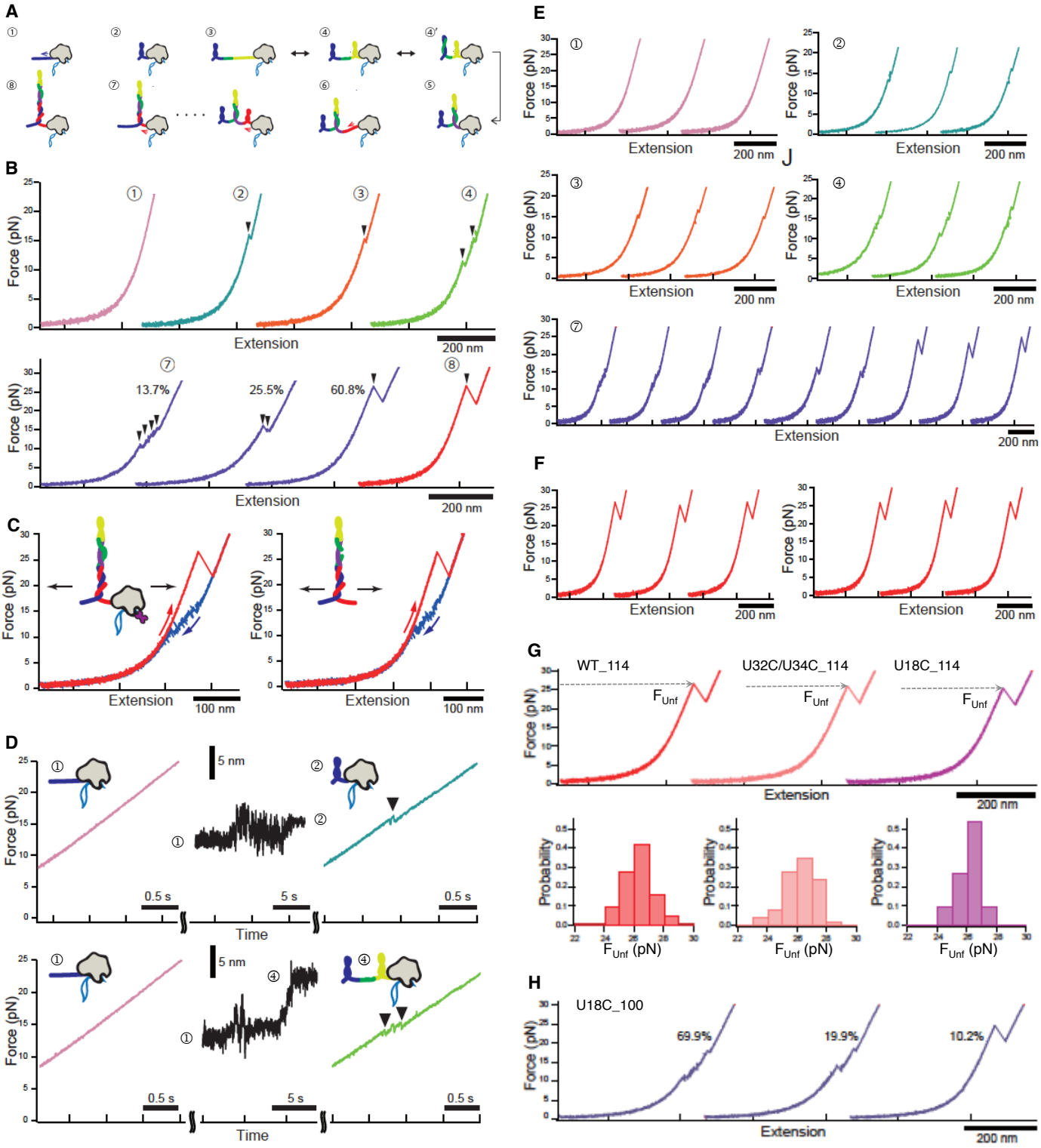
A
B
C
D
E
F
G
H
Force (pN)
Extension
200 nm
100 nm
13.7%
25.5%
60.8%
5 nm
0.5 s
5 s
Time
WT_114
U32C/U34C_114
U18C_114
F_Unf
F_Unf (pN)
Probability
U18C_100
69.9%
19.9%
10.2%

Figure S2

Figure S2. Force-Extension (F-X) Curve Measurements with Nascent RNA:RNAP Stalled Complexes to Characterize the Folding Progression of SRP RNA; Related to Figure 2, 3, and 5

(A) A schematic cartoon illustrates the folding intermediates of nascent SRP RNA as it is transcribed by RNAP (same as that shown in Figure 2E). In this study, six stalled RNA:RNAP complexes were examined. Specifically, the RNAP was stalled by a biotin:streptavidin roadblock located at six different base-pair positions on the template DNA: 40 bp (cartoon ① in Figure 2E), 52 bp (cartoon ②), 84 bp (cartoon ③), 97 bp (cartoon ④), 114+16 bp (cartoon ⑦), and 114+39 bp (cartoon ⑧), so as to incrementally lengthen the nascent RNA chain emerged on the RNAP surface. Since the RNAP footprint covers ~14-nt on the RNA transcript 3'-end (and ~27 bp on the template DNA), the lengths of RNAs outside of RNAP are estimated to be ~13-nt (=40-14-27/2; ①), ~25-nt (②), ~57-nt (③), ~70-nt (④), and ~103-nt (⑦), respectively. For the last complex (⑧), an additional 12 nt (=39-14-27/2) are appended to the full-length (114-nt) SRP RNA 3'-end, allowing sufficient separation from the RNAP surface.

(B) Representative force-extension (F-X) unfolding curves of incrementally lengthened nascent SRP RNA bound on RNAP: pink for complex ①, light green for complex ②, orange for complex ③, yellow green for complex ④, purple for complex ⑦ (which can access three competing folding states, as seen from the three different unfolding patterns; the relative distribution of those states are evaluated from a total number of n=153 F-X curves, recorded from 9 molecules), and red for complex ⑧, which is a full-length SRP RNA completely outside of the RNAP. Black arrowheads indicate where one or a series of unfolding events are detected along the F-X unfolding curves.

(C) Force-extension (F-X) curves (red, unfolding; blue, refolding) of full-length SRP RNA bound on RNAP (left panel) and of full-length SRP RNA isolated free in solution (right panel). In both cases, the full-length SRP RNA unfolds in one cooperative transition around 26 pN.

(D) Force-extension (F-X) curve measurements were also attempted co-transcriptionally (i.e. with actively transcribing RNA:RNAP complexes), so as to validate the RNA folding structure assignments for the nascent SRP RNA under possibly non-equilibrium conditions. Top panel: nascent RNA unfolding curves measured when transcription progresses from complex ① to ②, i.e. before the initial hump-like feature and after reaching the P1 pause in the co-transcriptional trace (middle trajectory in black, F=8.6 pN; see also Figure 2 and main text). The later F-X curve shows a small unfolding rip signature (black arrowhead), verifying the formation of H1 hairpin upon nascent RNA synthesis. Bottom panel: nascent RNA unfolding curves measured when transcription progresses from complex ① to ④, i.e. before the initial hump-like feature and after reaching the P2 pause in the co-transcriptional trace (middle trajectory in black, F=8.6 pN; see also Figure 2 and main text). The later F-X curve exhibits two small unfolding rips (black arrowheads), verifying that H1 and H2 hairpins readily form when half of the SRP RNA nascent chain has emerged from RNAP. The top and bottom sets of co-

transcriptional F-X curves were respectively obtained under depleting UTP (10 μM) and depleting GTP (10 μM) transcription conditions, so as to gain time for completing the measurements during the P1 and P2 pauses respectively.

(E) Additional representative F-X unfolding curves measured with complexes ①, ②, ③, ④, and ⑦ (same color-code as those shown in panel B) are shown to illustrate the consistency of F-X curve measurements across different molecules of the same nascent transcript length, and the reproducibility of the same molecule with repeating unfolding and refolding cycles. Total number of F-X curves recorded for complex ①: n=32 (from 12 molecules); complex ②: n=40 (from 12 molecules); complex ③: n=26 (14 molecules); complex ④: n=17 (7 molecules); and complex ⑦: n=153 (9 molecules). Complex ⑦, which bears a ~100-nt long nearly completed SRP RNA transcript, exhibits interchangeable unfolding patterns between unfolding cycles, signifying that this transcript stochastically populates/samples three accessible folding states. Note that these F-X curves are not displayed in the order of consecutive unfolding cycles, but rather in groups of similar unfolding patterns, so as to provide more examples for the unfolding of complex ⑦ unfolding shown in panel B. This observation illustrates that the nearly completed RNA attains competing structural folds, transitioning between intermediate states and the final long-hairpin native fold (i.e. the right-most unfolding curve that shows a large single-rip).

(F) Additional representative unfolding F-X curves measured with full-length SRP RNA bound on RNAP (left plot; total number of curves: n=110, from 10 molecules) and of full-length SRP RNA isolated free in solution (right plot; total number of curves: n=112, from 13 molecules).

(G) Representative unfolding F-X curves of full-length SRP RNAs (114-nt) containing wild-type sequence (WT_114), or one of the two mutant sequences (U32C/U34C_114 and U18C_114). All three RNAs unfold cooperatively in one transition, which pattern is consistent with a single long native hairpin fold as predicted by Mfold. Histograms of unfolding forces (F_{Unf}, marked by gray dash lines) measured with the respective full-length SRP RNAs listed above are also plotted (from left to right): the average unfolding force is 26.2±0.9 pN with WT_114 (total number of curves: n=110, from 12 molecules); 26.2±1.1 pN with U32C/U34C_114 (n=51, recorded from 12 molecules); and 26.1±0.8 pN with U18C_114 (n=41, recorded from 8 molecules).

(H) Representative unfolding F-X curves of near-completed SRP RNA transcript (100-nt) bearing the U18C mutation. Three types of unfolding patterns were detected (n=156): 10.2% is of one cooperative unfolding transition (*i.e.* a full-length like curve as the left most panel shown in Figure S6A); 19.9% is of two unfolding rips; and 69.9% is of several small consecutive unfolding rips. By contrast, the refolding curves (blue) appear similar and are indistinguishable among the three populations.

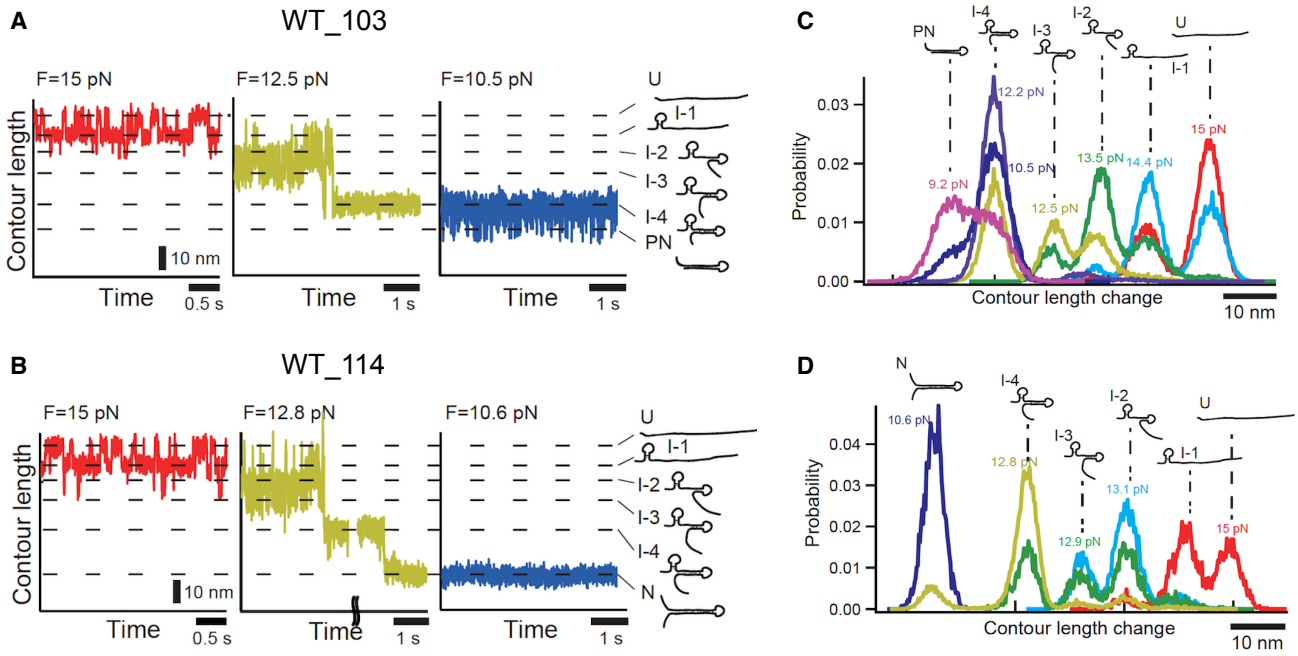
A
WT_103
F=15 pN
F=12.5 pN
F=10.5 pN
Contour length
10 nm
Time
0.5 s
1 s
U
I-1
I-2
I-3
I-4
PN
B
WT_114
F=15 pN
F=12.8 pN
F=10.6 pN
N
C
Probability
Contour length change
9.2 pN
10.5 pN
12.2 pN
12.5 pN
13.5 pN
14.4 pN
15 pN
D
10.6 pN
12.8 pN
12.9 pN
13.1 pN

Figure S3

Figure S3. Step-wise Folding Transition of Nearly-completed *vs.* Full-length SRP RNA: Transcript 3'-end Promotes the Attainment of Native Long-hairpin Fold; Related to Figure 2 and Figure 5

Step-wise folding transitions of wild-type SRP RNA—either nearly completed (103-nt, panel A) or as full-length (114-nt, panel B)—on the surface of RNAP (see also cartoon ⑥ & ⑧ in Figure 2E) are recorded using the force-clamp optical tweezers assay. In this assay, the tether is held at constant force and transitions between alternative folding states are recorded. Next, the applied constant force is reduced and the folding states accessible at the new force are recorded, and so on. Red traces obtained at 15 pN of tension, yellow traces at ~12 pN, and blue traces at ~10 pN. U: unfolded state; intermediate states: I-1 to I-4; PN: partial native state; N: native fold. Based on different extents of base-pairing in each structural fold, each folding state is characterized by a distinct tether end-to-end distance that is expressed in nm (dashed lines on y-axis in panel A and B, and on x-axis in panel C and D).

(A) Under 12.5 pN of clamping force (yellow), the 103-nt transcript transitions through intermediate states I-2, I-3, and I-1, and eventually stably adopts state I-4 (*i.e.* cartoon ⑥ in Figure 2E). When the clamping force further drops to 10.5 pN (blue), the transcript undergoes rapidly transitions between two competing folds, I-4 and PN (cartoon ⑦ in Figure 2E).

(B) For the full-length SRP RNA, similar folding transitions as that of the nearly-completed transcript are detected at clamping forces of 15 and ~12 pN, except that the 114-nt transcript can readily attain the native long hairpin fold (N) at 12.8 pN (yellow trace). At 10.6 pN, the full-length transcript exclusively adopts the native long hairpin fold.

(C-D) To construct the probability distributions of folded states visited by the SRP RNA as the clamping force decreases (panel C for 103-nt transcript, and panel D for 114-nt transcript), we integrate each force-clamping trace along the time axis and align them by the RNA tether contour length. The dominating population of native fold in panel D (dark blue peak) *vs.* the large population for the intermediate I-4 in panel C (dark blue peak), highlight that the last ~11 nt on the SRP RNA 3'-stretch facilitates the attainment of native long hairpin fold.

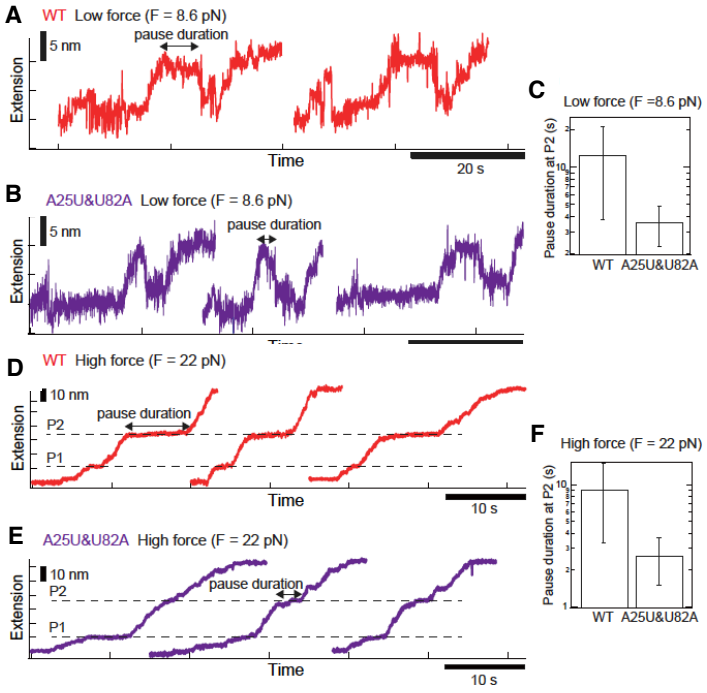
A
WT Low force (F = 8.6 pN)
pause duration
5 nm
Extension
Time
20 s
B
A25U&U82A Low force (F = 8.6 pN)
5 nm
pause duration
Extension
C
Low force (F =8.6 pN)
Pause duration at P2 (s)
WT A25U&U82A
D
WT High force (F = 22 pN)
10 nm
pause duration
P2
P1
Extension
Time
10 s
E
A25U&U82A High force (F = 22 pN)
10 nm
P2
pause duration
P1
Extension
Time
10 s
F
High force (F = 22 pN)
Pause duration at P2 (s)
WT A25U&U82A

Figure S4

Figure S4. Reduce P2 Pause in SRP RNA Transcription with Base-pairing Compensating Mutations U82A/A25U; Related to Figure 3

(A-B) Representative transcript extension traces with wild-type SRP RNA (WT) and A25U/U82A mutant. Real-time transcription recorded at 8.6 pN (low force condition) with 50 μM NTP.

(C) Mean pause duration at P2 site for transcription of wild-type SRP RNA (n=12) and A25U/U82A mutant (n=12), both recorded at low force condition ([NTP] = 50 μM).

(D-E) Representative transcript extension traces with wild-type SRP RNA (WT) and A25U/U82A mutant. Real-time transcription recorded at 22 pN (high force condition) and with 50 μM NTP.

(F) Mean pause duration at P2 site for transcription of wild-type SRP RNA (n=15) and A25U/U82A mutant (n=13), both recorded at high force condition ([NTP] = 50 μM).

A

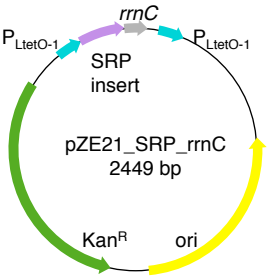

C

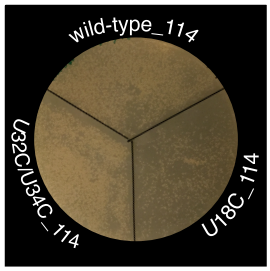

B Modifications in plasmids harbored in surviving colonies (n=5 for each)

SRP RNA variant	truncated/ impaired promoter (1st $P_{LtetO-1}$)	loss of SRP insert	truncated/ impaired terminator (rrnC)	termination read-through (2nd $P_{LtetO-1}$)
SRP_100	✔	✔	✔	✔✔✔✔
U18C_100	✔✔✔	✔✔	✔✔	✔✔
U32C/U34C_100	✔✔✔	✔✔✔✔	✔✔✔✔	✔✔

Figure S5

Figure S5. *In Vivo* Response toward SRP RNA Variant-carrying Plasmids; Related to Figure 5

(A) The plasmid construct of pZE21_SRP_rrnC, which is designed for precise transcription of SRP RNA variants inserted therein (see Methods for plasmid sequence). $P_{LtetO-1}$: a strong promoter (L for phage lambda), to which a *tet* operator is integrated within the promoter sequence so as to make it tightly repressible. This operator-embodying promoter avoids excessive/unwanted nucleotide sequence appended to the 5'-end of RNA product transcribed, which would be the case if a typical operator-appending promoter were used. *rrnC*: a strong terminator (Chen et al., 2013), immediately after the SRP RNA. Then a second $P_{LtetO-1}$ promoter located 54-nt downstream from the terminator. Binding of another RNAP to this second promoter serves as a roadblock to ensure that the first RNAP properly terminates on *rrnC*. Kan^R: kanamycin resistant. *ori*: high-copy-number colE1 origin of replication.

(B) Modifications of the above plasmid—such as impaired promoter, loss of SRP variant insert, and/or inefficient termination—were found in colonies surviving from the otherwise lethal transcription of SRP RNA truncated variants (Figure 5A, bottom half of the plate). Namely, these modifications compromise the precise transcription of the 3'-end-truncated SRP RNA variants and alleviate the toxic impact on cell viability.

(C) Under stress condition—*e.g.* high salt (2x Luria broth, *i.e.* 50g/L) and stiff growth medium (2x agar, *i.e.* 30g/L), as compared to normal LB agar plates (Figure 5), the difference in toxicity among plasmids carrying different full-length SRP RNA variants is further accentuated. Specifically, a greater reduction in surviving colonies is seen with the transformation of U18C_114 SRP RNA variant (lower right). Here, it shows ~28% colony counts relative to that of WT_114, compared to ~44% relative to that of WT_114 seen in Figure 5B.

NTP concentration	persistence length (nm)	conversion factor (nt/nm)
1 mM	1.31	2.77 (F = 8.6 pN)
50 uM	1.34	2.75 (F = 8.6 pN), 2.27 (F = 22 pN)
10 uM	1.39	2.71 (F = 8.6 pN)
nucleotide free	1.40	———————

Table S1. Persistence lengths of RNA and its conversion factors (nt/nm) under forces; Related to STAR Methods (section: Unit conversion of transcription trajectories recorded in nanometers into nucleotides)

Complete plasmid sequence of pZE21_wtSRP_FL_rrnC

Notations: ori (colE1) / Kan^R / $P_{LtetO-1}$ / wtSRP_FL / rrnC / **point mutation for U18C and U32C/U34C** / transcript truncation to 100-bp long

CTAGGCGTTCGGCTGCGGCGAGCGGTATCAGCTCACTCAAAGGCGGTAATACGGTTATC
CACAGAATCAGGGGATAACGCAGGAAAGAACATGTGAGCAAAAGGCCAGCAAAAGGCCA
GGAACCGTAAAAAGGCCGCGTTGCTGGCGTTTTTCCATAGGCTCCGCCCCCCTGACGAG
CATCACAAAAATCGACGCTCAAGTCAGAGGTGGCGAAACCCGACAGGACTATAAAGATA
CCAGGCGTTTCCCCCTGGAAGCTCCCTCGTGCGCTCTCCTGTTCCGACCCTGCCGCTTA
CCGGATACCTGTCCGCCTTTCTCCCTTCGGGAAGCGTGGCGCTTTCTCAATGCTCACGC
TGTAGGTATCTCAGTTCGGTGTAGGTCGTTCGCTCCAAGCTGGGCTGTGTGCACGAACC
CCCCGTTCAGCCCGACCGCTGCGCCTTATCCGGTAACTATCGTCTTGAGTCCAACCCGG
TAAGACACGACTTATCGCCACTGGCAGCAGCCACTGGTAACAGGATTAGCAGAGCGAGG
TATGTAGGCGGTGCTACAGAGTTCTTGAAGTGGTGGCCTAACTACGGCTACACTAGAAG
GACAGTATTTGGTATCTGCGCTCTGCTGAAGCCAGTTACCTTCGGAAAAAGAGTTGGTA
GCTCTTGATCCGGCAAACAAACCACCGCTGGTAGCGGTGGTTTTTTTGTTTGCAAGCAG
CAGATTACGCGCAGAAAAAAAGGATCTCAAGAAGATCCTTTGATCTTTTCTACGGGGTC
TGACGCTCAGTGGAACGAAAACTCACGTTAAGGGATTTTGGTCATGACTAGTGCTTGGA
TTCTCACCAATAAAAAACGCCCGGCGGCAACCGAGCGTTCTGAACAAATCCAGATGGAG
TTCTGAGGTCATTACTGGATCTATCAACAGGAGTCCAAGCGAGCTCTCGAACCCCAGAG
TCCCGCTCAGAAGAACTCGTCAAGAAGGCGATAGAAGGCGATGCGCTGCGAATCGGGAG
CGGCGATACCGTAAAGCACGAGGAAGCGGTCAGCCCATTCGCCGCCAAGCTCTTCAGCA
ATATCACGGGTAGCCAACGCTATGTCCTGATAGCGGTCCGCCACACCCAGCCGGCCACA
GTCGATGAATCCAGAAAAGCGGCCATTTTCCACCATGATATTCGGCAAGCAGGCATCGC
CATGGGTCACGACGAGATCCTCGCCGTCGGGCATGCGCGCCTTGAGCCTGGCGAACAGT
TCGGCTGGCGCGAGCCCCTGATGCTCTTCGTCCAGATCATCCTGATCGACAAGACCGGC
TTCCATCCGAGTACGTGCTCGCTCGATGCGATGTTTCGCTTGGTGGTCGAATGGGCAGG
TAGCCGGATCAAGCGTATGCAGCCGCCGCATTGCATCAGCCATGATGGATACTTTCTCG
GCAGGAGCAAGGTGAGATGACAGGAGATCCTGCCCCGGCACTTCGCCCAATAGCAGCCA
GTCCCTTCCCGCTTCAGTGACAACGTCGAGCACAGCTGCGCAAGGAACGCCCGTCGTGG
CCAGCCACGATAGCCGCGCTGCCTCGTCCTGCAGTTCATTCAGGGCACCGGACAGGTCG
GTCTTGACAAAAAGAACCGGGCGCCCCTGCGCTGACAGCCGGAACACGGCGGCATCAGA
GCAGCCGATTGTCTGTTGTGCCCAGTCATAGCCGAATAGCCTCTCCACCCAAGCGGCCG
GAGAACCTGCGTGCAATCCATCTTGTTCAATCATGCGAAACGATCCTCATCCTGTCTCT
TGATCAGATCTTGATCCCCTGCGCCATCAGATCCTTGGCGGCAAGAAAGCCATCCAGTT
TACTTTGCAGGGCTTCCCAACCTTACCAGAGGGCGCCCCAGCTGGCAATTCCGACGTCT
AAGAAACCATTATTATCATGACATTAACCTATAAAAATAGGCGTATCACGAGGCCCTTT
CGTCTTCACCTCGAGTCCCTATCAGTGATAGAGATTGACATCCCTATCAGTGATAGAGA
TACTGAGCACATCGGGGGCTCTGTTGGTTC**T**CCCGCAACGCTAC**T**C**T**GTTTACCAGGTC
AGGTCCGGAAGGAAGCAGCCAAGGCAGATGACGCGTGTGCCGGGATGTAGCTGGCAGGG

CCCCCACCCCAGATAAAAAAAATCCTTAGCTTTCGCTAAGGATGATTTCTCCTCGAGGT
CGACGGTATCGATAAGCTTGATATCGAATTCCTGCAGCGGATCCCATGGAGGCATTCCC
TATCAGTGATAGAGATTGACATCCCTATCAGTGATAGAGATACTGAGCACATCTTGCCA
TGTGTATGTGGGAGACGGTCGGGTCCAGATATTCGTATCTGTCGAGTAGAGTGTGGGCT
CCCACATACTCTGATGATCCTTCGGGATCATTCATGGCAATCTAGACAGATAAAAAAAA
TCCTTAGCTTTCGCTAAGGATGATTTCTAC